CrossMark

VLBI with SKA: Possible Arrays and Astrometric Science

Yingjie Li[1], Ye Xu[1,2], Jingjing Li[1], Shuaibo Bian[1], Zehao Lin[1], Chaojie Hao[1], and Dejian Liu[1,2]
[1] Purple Mountain Observatory, Chinese Academy of Sciences, Nanjing 210023, China; xuye@pmo.ac.cn, liyj@pmo.ac.cn
[2] University of Science and Technology of China, Hefei 230026, China

Abstract

The next generation of very long baseline interferometry (VLBI) is stepping into the era of microarcsecond (μas) astronomy, and pushing astronomy, especially astrometry, to new heights. VLBI with the Square Kilometre Array (SKA), SKA-VLBI, will increase current sensitivity by an order of magnitude, and reach astrometric precision routinely below 10 μas, even challenging 1 μas. This advancement allows precise parallax and proper motion measurements of various celestial objects. Such improvements can be used to study objects (including isolated objects, and binary or multiple systems) in different stellar stages (such as star formation, main-sequence stars, asymptotic giant branch stars, pulsars, black holes, white dwarfs, etc.), unveil the structure and evolution of complex systems (such as the Milky Way), benchmark the international celestial reference frame, and reveal cosmic expansion. Furthermore, the theory of general relativity can also be tested with SKA-VLBI using precise measurements of light deflection under the gravitational fields of different solar system objects and the perihelion precession of solar system objects.

Key words: astrometry – parallaxes – stars: kinematics and dynamics – ISM: kinematics and dynamics – Galaxy: kinematics and dynamics – galaxies: kinematics and dynamics – gravitation

1. Introduction

Astrometry focuses on how to measure the positions and motions of celestial objects as accurately as possible. The history of astrometry originates from the earliest astronomical observations recorded more than 2000 yr ago. Successive improvements in astrometric technology have increased the angular accuracy, leading to a number of important discoveries, such as Earth nutation and the proper motions, aberrations, and trigonometric parallaxes of stars. Such improvements have enhanced marine and aerospace navigation after the international celestial reference frame (ICRF) was established, based on accurate positional measurements of a large number of celestial bodies (Perryman 2012). The application of astrometry has continuously extended, from the solar system, to the whole Milky Way (MW), to galaxies, and the entire visible universe; the development of theories that depend on precise astrometry, such as heliocentric theory, Newtonian spacetime, and the theory of general relativity (GR), has occurred concurrently.

The history of astrometry is closely associated with that of stellar catalogs, because they offer reference points on the sky for astronomers to trace the motion of stars. In the 1830s, the first trigonometric parallax of a star was measured after many unsuccessful attempts (Bessel 1838), which opened up a new era of trigonometric parallax measurements. Over the past 400 yr, the accuracy of positional measurements has increased almost logarithmically with time. This increase of accuracy has allowed astronomers to quantify the extremely large scale of

the universe, determine the physical properties of stars, and ultimately describe the structure, dynamics, and the origin of our MW galaxy (for more details about the history of astrometry see Perryman 2012).

Astronomical observations in the radio started in the 1920s with Karl Jansky, and was further driven by the development of radar during World War II (Reid & Honma 2014). The earliest realization of applying interferometric techniques to practical astronomical observation dates back to the 1920s, when the first two-element optical interferometer was used (Thompson et al. 2017). The technique of two-element interferometry was applied to astronomical radio observations in the 1940s (Ryle & Vonberg 1946), and the realization of voltage multiplier correlators dates back to 1952 (Thompson et al. 2017).

Since the middle of the 20th century, radio and space optical astrometry has developed side by side, providing mutual reinforcement, ushering in breakthroughs in astrometry. In the 1950s–1960s, radio interferometric techniques continuously improved, increasing astrometric accuracy continuously from $\sim 1''$ to $0.''03$ (Wade & Johnston 1977). In the late 1960s, the use of precise atomic clocks and magnetic tapes to record data made it possible to overcome baseline length limitations by not having to transfer radio signals directly through cables, which eventually revolutionized radio interferometry. This new technology was dubbed very long baseline interferometry (VLBI; Reid & Honma 2014), and the first successful radio VLBI was in 1967 (Thompson et al. 2017). During the middle

of the 1970s, different facilities were tied together to form arrays with more than 10 elements. In this early stage of VLBI, the absolute positional accuracy was better than ∼0.3 mas (Clark et al. 1976; Ma et al. 1986), and relative astrometric accuracy between fortuitously close pairings of quasi-stellar objects (QSOs) reached ∼10 μas (Marcaide et al. 1985).

With improvements in positional precision, GR effects gradually became obvious and affected the precision of astrometry. For instance, from GR predictions, light should be deflected by ∼500 mas if it passes within 1° of the Sun, and the maximum deflection angle caused by Jupiter exceeds ∼16 mas (e.g., Li et al. 2022c). In the 1980s, GR models for light propagation began to be applied to VLBI observations, and a "consensus model" was published in 1991 (see Eubanks 1991; Petit & Luzum 2010). Currently, the relative time delays between antenna pairs caused by the Sun, the planets, the Moon, and the large satellites of Jupiter, Saturn, and Neptune are determined using data correlators, which are equivalent to deducting the deflection angles caused by the corresponding lenses (see, e.g., Petit & Luzum 2010). The use of data correlators has further enhanced high-precision astrometry.

In the same year as the first successful radio VLBI observation, it was proposed that precise measurements of triangular parallax from space could be achieved. This assertion was made a reality with the launch of the optical satellite Hipparcos (launched in 1989 August and ceased operation in 1993 March). Before the middle of the 1990s, the number of stars that had parallax measurements made by ground facilities was only ∼8000 (van Altena et al. 1995). The Hipparcos satellite provided the positions, parallaxes, and proper motions of approximately 120,000 stars with high accuracy (i.e., up to ∼1 mas, ESA 1997, although this accuracy was inferior to the accuracy of radio VLBI measurements). Later catalogs included the Tycho 2 catalog (see Høg et al. 2000) containing 2.5 million stars with improved astrometric quality, albeit mainly for the brightest stars (van Leeuwen 2010). Ever since radio VLBI and the Hipparcos satellite determined the positions of celestial objects, comparisons between optical and radio astrometry have been carried out. The most prominent example is the comparison between the optical and radio reference frames. Eventually, the VLBI-based ICRF (i.e., ICRF1, Ma et al. 1998) was adopted by the International Astronomical Union (IAU) in 1995. In this era, a controversy existed between the optical and radio reference frames, and there was more to it than that, such as the famous "Pleiades distance controversy" (Melis et al. 2014). In this controversy, the parallax obtained by the Hipparcos satellite was different from the distance obtained by other methods, including parallax measurement by VLBI. It has been described as "one of the more dramatic controversies in modern astrophysics" (Paczynski 2003).[3]

The first array of antennas built specifically for astronomical VLBI measurements was the Very Long Baseline Array, VLBA, of the National Radio Astronomy Observatory,[4] which began operations in 1994 (Thompson et al. 2017). A VLBI dedicated to astrometry, and more specifically, to obtain a three-dimensional (3D) map of the MW galaxy, is the Japanese VLBI Exploration of Radio Astrometry (VERA), which has been under regular operation since the fall of 2003.[5] Stepping into the 2000s, with the improvement of calibration techniques used in VLBI, a relative position accuracy of ∼10 μas was routinely achieved for most bright targets (Reid & Honma 2014), including a record parallax precision of ±5 μas (Zhang et al. 2013). Contemporaneously, Gaia, as the successor to the Hipparcos space astrometry project, was launched in 2013. To date, there have been three data releases from Gaia (i.e., DR1, DR2, and (E)DR3; Gaia Collaboration et al. 2016, 2021, 2023). At present, Gaia's astrometric accuracy is 20–30 μas, and is expected to reach ∼7 μas in Data Release 5. The first priority of Gaia was to address the "Pleiades distance controversy" (Gaia Collaboration et al. 2016). Gaia DR2 successfully ended the controversy, finding a distance consistent with that obtained by other methods including VLBI triangular parallax measurements (a summary of distance measurements is given in Lodieu et al. 2019).

VLBI and Gaia astrometry have had a profound effect on many fields in astronomy. Two important areas of comparative research are the comparison of the optical and radio reference frames and the study of the structure of the MW, which are still active today. In the long-term comparison of the optical and radio reference frames, notable VLBI-Gaia positional offsets, i.e., offsets between measured optical and radio positions, have been discovered. Specifically, these offsets are found in the positions in the most recent, third release of the ICRF, (ICRF3; Charlot et al. 2020), and from the Gaia Celestial Reference Frame (GCRF) based on EDR3 (Gaia Collaboration et al. 2022). The precision of Gaia astrometry is constantly improving, and solving these VLBI-Gaia positional offsets also requires a continual improvement of radio VLBI positional precision and spatial resolution as well as multiband radio and multiple calibrator observations.

The structure of the MW cannot be studied by the data produced by Hipparcos, because the distances of stars that could be accurately determined was limited to ∼100 pc in the Tycho-2 star catalog (ESA 1997). The accurate measurement of the distance to the high-mass star-forming region (HMSFR) W3(OH) using VLBA (with a parallax accuracy up to 0.01 mas; Xu et al. 2006), marked the possibility of making direct measurements of the spiral arm structure of Galaxy, opening a

---

[3] See https://www.cosmos.esa.int/web/Hipparcos/pleiades-distance.

[4] The National Radio Astronomy Observatory is a facility of the US National Science Foundation operated under cooperative agreement by Associated Universities, Inc.

[5] See https://www.miz.nao.ac.jp/veraserver/.

new era in the study of the structure of the MW. At present, precise triangular parallaxes have been measured for over 200 masers associated with HMSFRs in the Bar and Spiral Structure Legacy (BeSSeL) survey[6] (Brunthaler et al. 2011) and the VERA project (see footnote 5) (VERA Collaboration et al. 2020). These surveys have achieved fruitful results, such as mapping the nearest spiral arm, the Local arm, in unprecedented detail (Xu et al. 2013, 2016), generating the most complete spiral arm structure pattern of the MW to date (Reid et al. 2019b). Data from Gaia can densify the pattern of the spiral structure of the MW near the Sun (within ∼5 kpc) and even allow investigations of the evolution of its spiral structure. For instance, the structures traced by young OB stars are consistent with those traced by masers associated with HMSFRs (e.g., Xu et al. 2018a, 2018b, 2021b). Additionally, the large age spans of open clusters made them suitable for studying the motion and evolution of spiral arms (e.g., Hao et al. 2021), and even main-sequence stars and old stars can be used to constrain spiral arm structure (e.g., Poggio et al. 2021; Lin et al. 2022).

The comprehensive utilization of high-precision astrometric data from VLBI and Gaia has promoted research on the structure and evolution of the MW, but there are still some issues that need to be solved. For example, using high-precision data of various young stellar objects (YSOs, including masers, OB stars and young open clusters), Xu et al. (2023) proposed a new model of Galactic spiral arm that appears to be different from the previous mainstream view depicted by Georgelin & Georgelin (1976) and Reid et al. (2019b). However, there is still a lack of sufficient data to depict the spiral structure across the southern sky and beyond the Galactic center (GC). Will the spiral arm structure traced by masers still be consistent with that traced by OB stars (see Xu et al. 2021b)? Is the formation of stars in the spiral arms uneven (Xu et al. 2021b)? These questions may be answerable with the next generation of radio telescopes.

The next generation of instruments, such as the Square Kilometre Array (SKA; including SKA-Mid and SKA-Low; Braun et al. 2015), will greatly improve sensitivity (by an order of magnitude) and cover a wide range of frequencies from dozens of MHz to dozens of GHz. The concept of VLBI with the SKA (SKA-VLBI) was introduced for the first time in Paragi et al. (2015). SKA-VLBI is about phasing up the core of SKA telescopes, providing multiple tied-array beams that would target a number of sources within the primary field of view (FoV) of the antennas that form a VLBI array together with the SKA. The Karl G. Jansky Very Large Array (JVLA) in the USA (as part of the High Sensitivity Array, HSA) and the Westerbork Synthesis Radio Telescope in the Netherlands (formerly part of the European VLBI Network, EVN) provided a single tied array beam in the past; what is new in SKA-VLBI

is that it adds a very sensitive component to VLBI networks with large-FoV and multi-beam capability.

The large-FoV will enable SKA-VLBI to offer the multiple in-beam sources astrometry approach (Fomalont & Reid 2004). This has been done with different arrays (VLBA, EVN), albeit typically using only one calibrator. The great benefit is that it allows for simultaneous observation of the target source and calibrators. Moreover, the major improvement in precision can be achieved with a number of in-beam sources that individually not, but when their signal is combined they do reach dynamic ranges (DR) of ∼100:1. Another advanced technology is using multiple bright calibrators in the sky at several degrees apart, and fit for a phase-screen across the sky, which is called MultiView (Fomalont & Kopeikin 2003; Fomalont 2005; Rioja & Dodson 2020). Both methods will already help removing the bulk of the systematics, although it is true that the final astrometric precision will depend on various factors (like the brightness, compactness, the number, and the distribution of these calibrators) and may reach routinely below 10 μas, even challenging 1 μas. It should be noted that extremely high-precision astrometry (e.g., SKA μas astrometry) will face the challenge of light deflection under the gravitational fields of celestial bodies in the solar system (e.g., Li et al. 2022b). In any case, there is now a realistic possibility of carrying out μas radio astrometric surveys of exquisite detail for large samples of objects, which will advance our understanding of different astrophysical phenomena and classes (Rioja & Dodson 2020).

Paragi et al. (2015) described motivation for and the possible realization of SKA-VLBI. This paper will give an extensive review of possible astrometric science with SKA-VLBI. The remainder of this paper is organized as follows. Section 2 describes which telescopes/sites can be used to make up VLBI arrays or networks with SKA-Mid, and their corresponding sensitivities and astrometric precision. Due to a variety of target sources, it is difficult to cover all the scientific subjects that can be carried out in a single study. However, we use a point to point narrative to gradually depict SKA-VLBI astrometric science in Section 3. We divide the achievable science into astrometry of isolated objects in Section 3.1; of binary and complex systems in Sections 3.2 and 3.3; and tests of GR in Section 3.4. Finally, Section 4 gives a summary.

2. Possible VLBI Networks for SKA-Mid

2.1. The Compositions of Possible VLBI Networks

The main focus of this work is astrometry, and the lowest frequency considered in this work is ∼1 GHz. Due to the frequency of the three priority bands currently planned for deployment for SKA-Mid (950–1760, 4600–8500, and 8300–15,300 MHz),[7] the frequency ranges considered in this work are 1.0–2.0 GHz and 4.6–15.3 GHz. They are further

---

[6] See http://bessel.vlbi-astrometry.org.

[7] See https://skao.canto.global/s/MH29C?viewIndex=0.

Figure 1. The sites in this work, plotted using an ovital map (see https://www.ovital.com/). SKA-Mid is labeled as "SKA_M."

divided into eight bands, i.e., bands L1, L2, C1, C2, C3, X, Ku1, and Ku2 centered at 1.3, 1.6, 5.0, 6.0, 6.7, 8.0, 12.0, and 15.0 GHz, respectively.

Currently, the common radio interferometry arrays or networks operating at ∼1–15 GHz include the VLBA and JVLA in the USA, the EVN, the East Asia VLBI Network (EAVN), the Australian Long Baseline Array (LBA), the upgraded Giant Metrewave Radio Telescope (uGMRT) in India, etc. Some subarrays of these arrays or networks (which can work independently) include the Multi-Element Radio Interferometer Network (MERLIN) in the UK, the Korean VLBI Network (KVN), the Japanese VLBI Network (JVN), VERA, and the Chinese VLBI Network (CVN), etc. Large single dishes include the Five-hundred-meter Aperture Spherical radio Telescope (FAST) in China, the Green Bank Telescope (GBT) in the USA, and Effelsberg (EFS) in Germany, etc. Telescope arrays or single dishes under development or construction include the SKA (including SKA-Mid and SKA-Low), next-generation Very Large Array (ngVLA), the African VLBI Network (AVN), Jingdong in

China, etc. The total number of telescopes and/or tied arrays involved in this work is 82 (their distribution can be seen in Figure 1 updated on 2023 April 1). These facilities have the potential to be used in VLBI arrays or networks with SKA-Mid. Table A1 lists the basic parameters of these telescopes, such as their geographical position, aperture, and system equivalent flux density (SEFD). Figure 2 shows which telescopes or arrays may be able to form VLBI arrays or networks with SKA-Mid in various bands.

SKA-Mid is suitable for observing sources with decl. (J2000) below ∼35°, assuming source elevations greater than 20°. In this work, the scenarios we analyze include sources with decl. of −50°, −35°, −20°, −5°, 10°, 25°, and 35°. Considering that not all telescopes that can observe in a certain band can simultaneously observe a source with a specific decl. (J2000), we divided them into different groups based on UTC time. We showed at most two groups in this work, and more groups can be drawn from Figure 2 and the distribution of elevation of each telescope (see an example in Figure 3). Figure 4 displays examples of uv coverage in band C1 for two

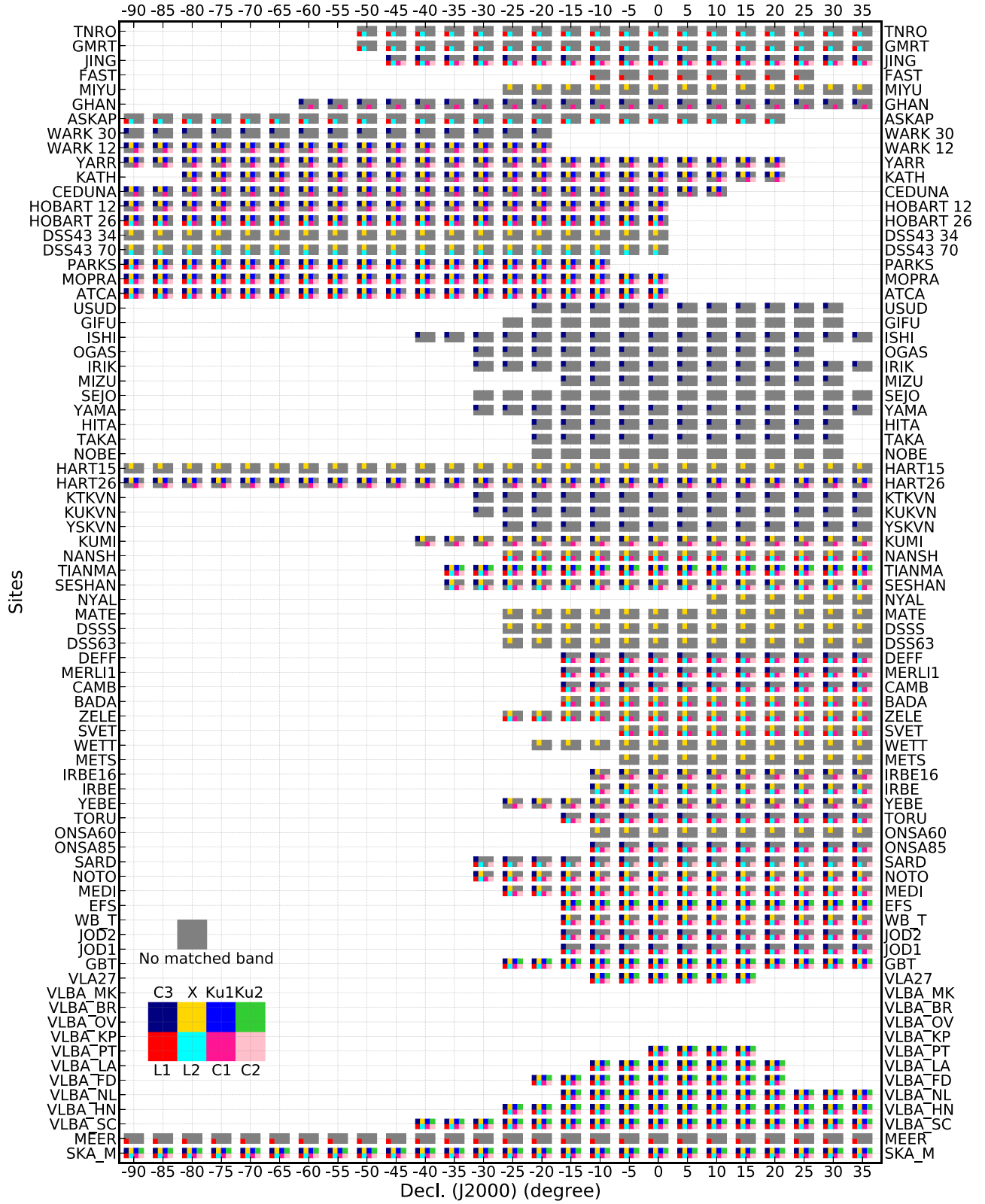**Figure 2.** The potential sites of SKA-VLBI for target sources with different decl. (J2000), where L1, L2, C1, C2, C3, X, Ku1, and Ku2 represent different bands. SKA-Mid is labeled as "SKA_M."
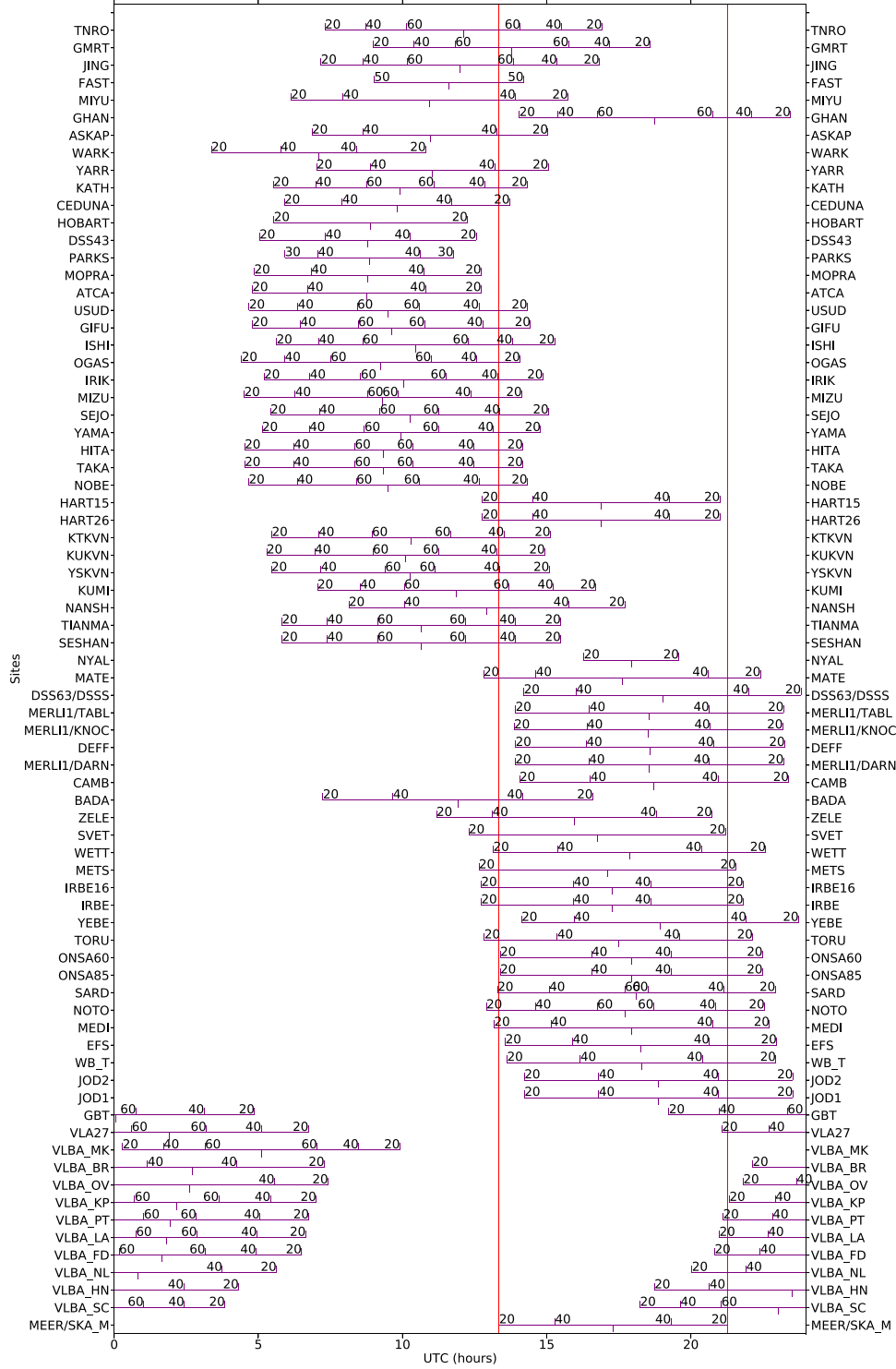
Figure 3. The distribution of elevation for target sources with decl. (J2000) of $10°$. The red vertical lines indicate the UTC time range with the elevation of SKA-Mid (which is labeled as "SKA_M") being $20°$.
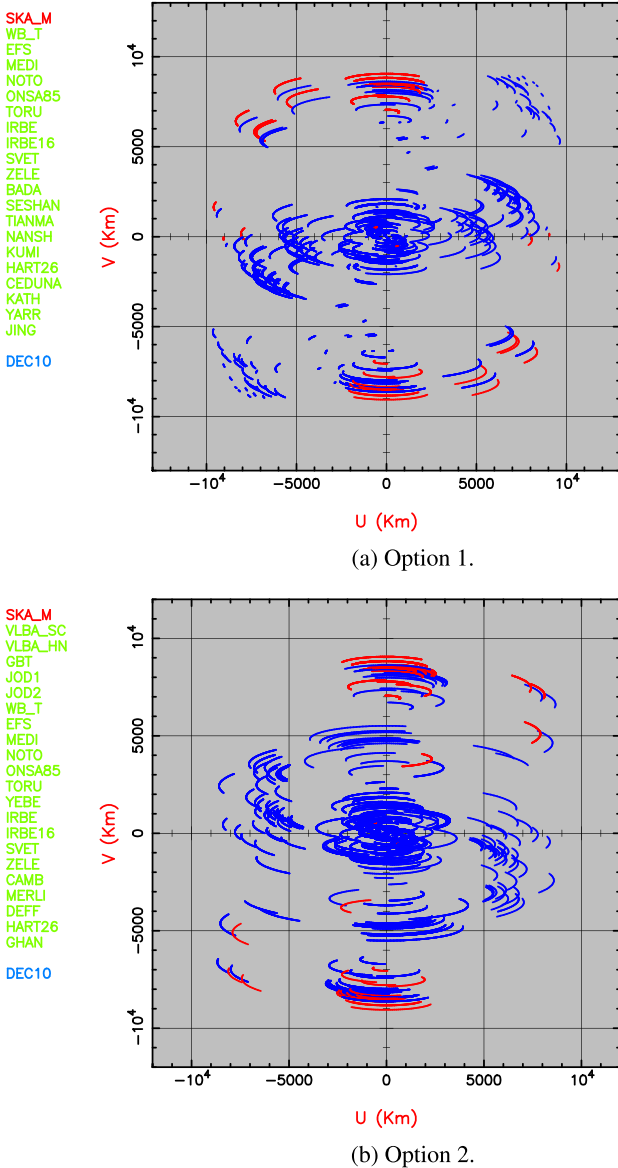
(a) Option 1.

(b) Option 2.

Figure 4. Map of uv coverage in band C1 for options 1 (panel (a)) and 2 (panel (b)), with target sources' decl. (J2000)=10°. The uv coverage was mapped with the tool provided at http://www.aoc.nrao.edu/software/sched/.

groups with decl. of target source being 10°, where the sites involved in each case are also listed. Table 1 lists the corresponding shortest and longest baseline lengths between each site and SKA-Mid. A subclass of facilities able to measure OH (labeled as L_OH) is also included, because OH masers are important tracers in astronomy. For example, OH masers at 1612/1665/1667 MHz trace diverse physical processes such as star-forming regions and evolved stars (e.g., Fish & Reid 2007; Beuther et al. 2019), and magnetic fields (e.g., Fish et al. 2005; Fish & Reid 2006; Crutcher et al. 2010). The 6.7 GHz methanol maser is an important tracer of HMSFRs (e.g.,

Ellingsen 2006; Green et al. 2009; Yang et al. 2019) and the structure of the MW (e.g., Xu et al. 2016; Reid et al. 2019b; Li et al. 2022a). Figure 5 plots the distribution of the baseline lengths of all sites against the SKA-Mid. Most baselines exceed ∼8000 km, the maximum length is ∼12,000 km, and the typical value is ∼10,000 km.

2.2. Sensitivity and Astrometric Precision Possible with SKA-VLBI

For each pair of antennas, their combined SEFD_{ij} is

$$\mathrm{SEFD}_{ij} = \sqrt{\mathrm{SEFD}_i \times \mathrm{SEFD}_j}, \tag{1}$$

where subscripts i and j represent the ith and jth telescopes, respectively. The total SEFD of an array is read as

$$\mathrm{SEFD} = \frac{1}{\sqrt{\sum_{i,j=1}^{n;i<j} \frac{1}{\mathrm{SEFD}_i \times \mathrm{SEFD}_j}}}, \tag{2}$$

and the sensitivity for single polarization without considering the effect of sampling is

$$\Delta S = \frac{\mathrm{SEFD}}{\eta_s} \sqrt{\frac{1}{2 \times \Delta \nu \times \tau_{ff}}}, \tag{3}$$

where $\Delta \nu$ is the bandwidth, which is set to 128 MHz for the L band (including L1 and L2) and 256 MHz for the other bands (i.e., the same as in Rioja & Dodson 2020); τ_{ff} is the integration time, which is set to 1 hr; and η_s is set to 0.7, i.e., the same as in "EVN Calculator."[8]

In order to calculate the sensitivity under various conditions, Table 2 lists the SEFDs corresponding to the cases in Table 1. Considering that only the inner 4 km core may be phased up, we expect SEFD of SKA-MID to be ∼2.6 Jy at ∼1–8 GHz (Paragi et al. 2015, see more details in Table A1). With respect to L2, there are two more telescopes that can observe L_OH, i.e., the MEER (the upper frequency limit of its L band is 1670 MHz, and the lower limit of its S band is 1750 MHz) and HART26 (the lower frequency limit of its L band is 1608 MHz). The mean SEFDs listed in Table 2, i.e., the row labeled "mean," were adopted to calculate the corresponding sensitivity of each band (i.e., L1, L2, C1, C2, C3, X, Ku1, and Ku2 at 1.3, 1.6, 5.0, 6.0, 6.7, 8.0, 12.0, and 15.0 GHz, respectively), using Equation (3).

The position measurement uncertainty (i.e., astrometric precision) reads (Reid et al. 1988; Condon 1997)

$$\Delta \theta \approx 0.5 \frac{\theta_{\mathrm{beam}}}{\mathrm{DR}} \approx 0.5 \frac{\lambda}{b} \frac{1}{\mathrm{DR}}, \tag{4}$$

where $\theta_{\mathrm{beam}} \approx \lambda/b$ is the full width at half maximum (FWHM) of the beam, b is the baseline length, and λ is the wavelength. Here, b is set to 10,000 km, because the baseline lengths linked to SKA-Mid are mostly around this length (Table 1). Table 3

---

8 See https://services.jive.eu/evn-calculator/cgi-bin/EVNcalc.pl.

Table 1
Shortest and Longest Baseline Lengths versus SKA-Mid

Decl. (°)	L1 (km)	L2 (km)	L_OH (km)	C1 (km)	C2 (km)	C3 (km)	X (km)	Ku1 (km)	Ku2 (km)	Comment
					Option 1					
−50	(7382, 9892)	(7382, 9892)	(811, 9892)	(811, 10351)	(811, 10351)	(811, 10351)	(811, 10351)	(811, 10351)	...	a
−35	(7382, 10608)	(7382, 10612)	(811, 10612)	(811, 10612)	(811, 10612)	(811, 10612)	(811, 10612)	(811, 10608)	...	b
−20	(7382, 10608)	(7382, 10612)	(811, 10612)	(811, 10612)	(811, 10612)	(811, 11542)	(811, 10612)	(811, 10608)	(9443, 11709)	c
−5	(7382, 10608)	(7382, 10612)	(811, 10612)	(811, 10612)	(811, 10612)	(811, 11578)	(811, 10632)	(811, 10608)	(8349, 11709)	d
10	(7080, 10608)	(7080, 10612)	(811, 10612)	(811, 10612)	(811, 10612)	(811, 11578)	(811, 10632)	(811, 10608)	(8349, 11887)	e
25	(7080, 10608)	(7080, 10612)	(811, 10612)	(811, 10612)	(811, 10612)	(811, 11578)	(811, 10632)	(811, 11358)	(8349, 11358)	f
35	(7080, 10608)	(7080, 10612)	(811, 10612)	(811, 10612)	(811, 10612)	(811, 11147)	(811, 10632)	(811, 11358)	(8349, 11358)	f
					Option 2					
−50	...	...	...	...	...	...	...	...	...	...
−35	...	...	...	(811, 9443)	...	(811, 9443)	...	...	...	g
−20	(7080, 7879)	(7080, 7879)	(811, 7879)	(811, 7879)	(811, 7791)	(811, 7791)	(811, 8177)	(9443, 11709)	...	h
−5	(7080, 9411)	(7080, 9411)	(811, 9411)	(811, 9439)	(811, 9439)	(811, 9439)	(811, 9439)	(9443, 11709)	(9443, 11869)	i
10	(7080, 10839)	(7080, 10839)	(811, 10839)	(811, 10839)	(811, 10839)	(811, 10839)	(811, 10839)	(8349, 11887)	...	j
25	(7080, 10839)	(7080, 10839)	(811, 10839)	(811, 10839)	(811, 11358)	(811, 11358)	(811, 10839)	...	...	j
35	(7080, 11358)	(7080, 11358)	(811, 11358)	(811, 11358)	(811, 11358)	(811, 11358)	(811, 11358)	...	...	j

Note. L_OH is added to denote the bands that can observe 1612/1665/1667 MHz OH masers.
[a] Mainly in Africa and Oceania.
[b] In Africa, Oceania, and Asia.
[c] In Africa, Oceania, and Asia in bands L1–Ku1, and in Africa and North America in band Ku2.
[d] In Africa, Oceania, and Asia in bands L1–Ku1, and mainly in Africa and North America in band Ku2.
[e] Mainly in Africa, Oceania, and Asia in bands L1–X; in Africa, Oceania, Asia, and Europe in band Ku1; and mainly in Africa and North America in band Ku2.
[f] Mainly in Africa, Europe, and Asia in bands L1–X, and mainly in Africa and North America in bands Ku1 and Ku2.
[g] In Africa and North America (only four sites).
[h] Mainly in Africa and Europe in bands L1–X, and in Africa and North America in band Ku1.
[i] Mainly in Africa, Europe, and North America in bands L1–X, and in Africa and North America in bands Ku1 and Ku2.
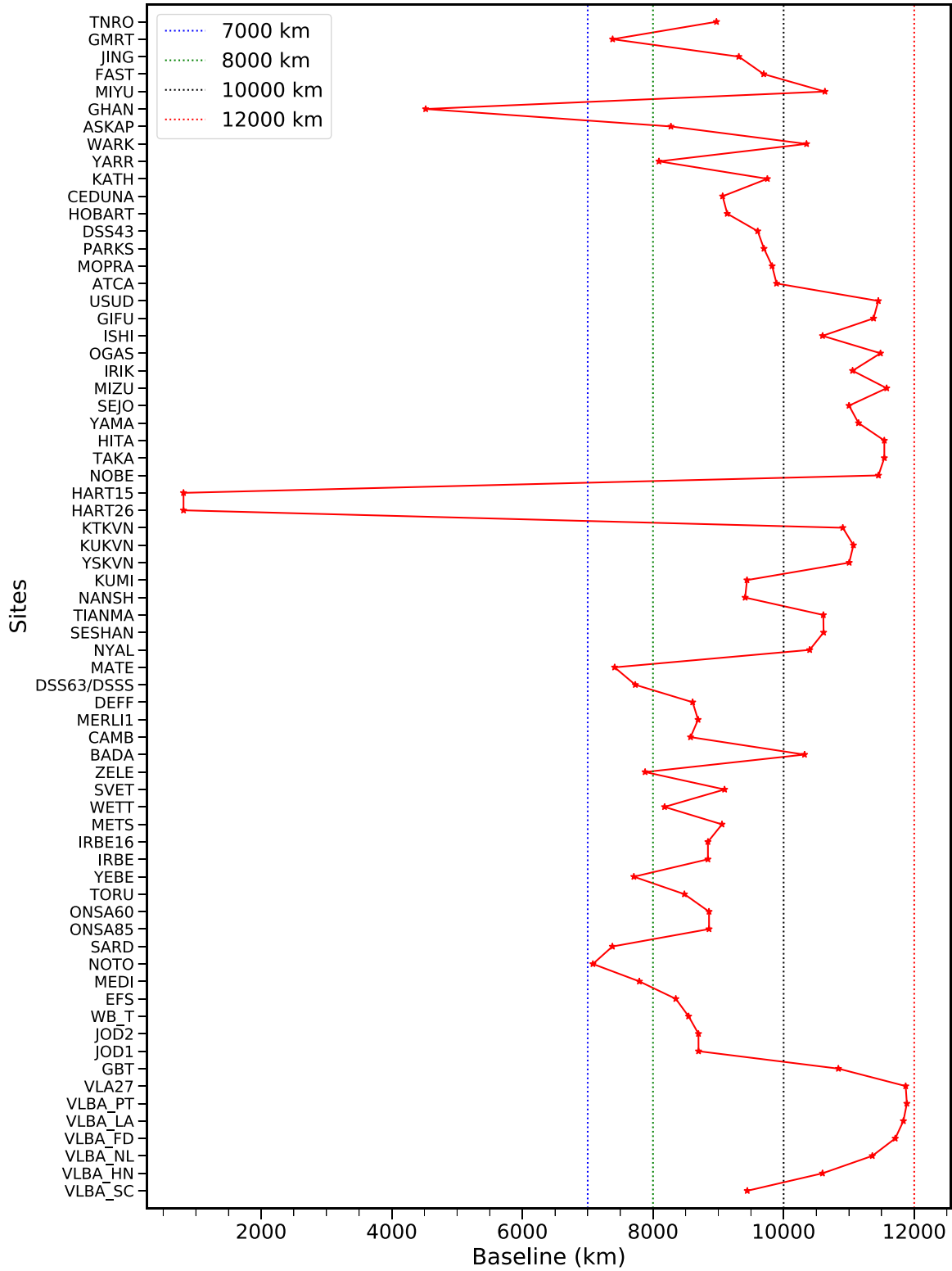[j] Mainly in Africa, Europe, and North America.

Figure 5. Distribution of the baseline lengths of all sites against SKA-Mid. The blue, green, black and red vertical lines indicate baselines of 7000, 8000, 10,000 and 12,000 km, respectively.

Table 2
SEFDs of Possible SKA-VLBI Arrays

Decl. (°)	L1 (Jy)	L2 (Jy)	L_OH (Jy)	C1 (Jy)	C2 (Jy)	C3 (Jy)	X (Jy)	Ku1 (Jy)	Ku2 (Jy)
Option 1									
−50	2.8	3.3	2.5	8.4	8.9	10.3	4.9	17.7	⋯
−35	1.9	2.1	1.8	3.0	3.1	3.3	4.3	11.2	⋯
−20	1.9	2.1	1.8	3.0	3.1	3.1	4.2	11.2	8.3
−5	1.2	2.2	1.8	3.0	3.1	3.2	4.4	11.8	7.2
10	1.1	2.1	1.7	2.6	2.7	2.7	4.4	10.6	4.6
25	1.0	1.5	1.4	2.0	2.0	2.0	3.3	7.3	7.4
35	1.5	1.5	1.4	2.0	2.0	2.1	3.3	7.3	7.4
Option 2									
−50	⋯	⋯	⋯	⋯	⋯	⋯	⋯	⋯	⋯
−35	⋯	⋯	⋯	17.9	⋯	19.5	⋯	⋯	⋯
−20	3.1	4.5	3.1	10.7	9.3	9.0	5.2	8.3	⋯
−5	1.5	1.6	1.4	2.1	2.2	2.2	3.7	7.2	4.9
10	1.9	2.0	1.7	2.3	2.4	2.4	3.0	4.6	⋯
25	1.6	1.7	1.5	2.3	2.4	2.4	3.0	⋯	⋯
35	1.6	1.7	1.5	2.3	2.4	2.4	2.9	⋯	⋯
mean[a]	1.8	2.2	1.8	3.6	3.6	3.8	3.9	9.7	6.6

Note.
[a] The case of −35° in option 2 is not included.

Table 3
Characterizing SKA-VLBI Astrometry

Frequency (GHz)	SEFD (Jy)	ΔS (μJy beam^{-1})	$\theta_{\rm beam}$ (mas)	$\Delta\theta$ (μas)	No. of In-beam Sources
1.3	1.8	2.7	4.8	24	53.1
1.6	2.2	3.3	3.9	19	27.7
5.0	3.6	3.8	1.2	6	1.5
6.0	3.6	3.8	1.0	5	1.0
6.7	3.8	4.0	0.9	5	0.7
8.0	3.9	4.1	0.8	4	0.5
12.0	9.7	10.2	0.5	3	0.1
15.0	6.6	6.9	0.4	2	0.1

Note. Assuming the baseline length is 10,000 km and the typical telescope aperture is 32 m. For ΔS, the integration time is 1 hr, where the bandwidth is 128 MHz for the L band and 256 MHz for the other bands.

lists the astrometric precision for DR of 100:1. Note that parallax precision will be 3–5 times better or even better than the astrometric precision with multiepoch observations (e.g., Xu et al. 2006, 2013; Deller et al. 2019). In this work, the parallax precision is assumed to be 1/3 of the astrometric precision.

We calculated the number of in-beam sources, similar to Rioja & Dodson (2020). The FoV is (Thompson et al. 2017)

$$\text{FoV} \approx \frac{\lambda}{d}, \qquad (5)$$

where λ is the wavelength and d is the aperture, which here is fixed to 32 m because most telescopes have an aperture below 32 m (see Table A1). Using the tiered radio extragalactic continuum simulation of the continuum radio sky in Bonaldi et al. (2019), we can estimate the number of sources that can be detected under different flux densities levels. Their simulations included active galactic nuclei (AGNs) and star-forming galaxies (SFGs), and the number of sources counted in this work includes both objects. In their simulations they only consider frequencies of 1.4, 1.9, 5.0, 6.7, 9.2, 12.5, and 20.0 GHz. Therefore, the calculations in the current work at 1.3 and 1.6 GHz are based on the simulation results at 1.4 GHz, while those at 6.0, 8.0, 12.0, and 15 GHz are based on simulated frequencies of 6.7, 9.2, 12.5 and 12.5 GHz, respectively (see Figure 6). The numbers of in-beam sources are listed in Table 3. It is feasible to find multiple in-beam calibrators at L band.

3. Astrometric Science with SKA-VLBI

The astrometry of SKA-VLBI will be characterized by high sensitivity and high precision. This section describes some of the astrometric science that can be conducted with SKA-VLBI. The important measurement quantities of astrometry are parallax and proper motion, with which one can obtain 5D (traced by continuum emission) or 6D (combining radial velocities traced by masers) information to study the physical and dynamical properties of target sources. Such objects can be
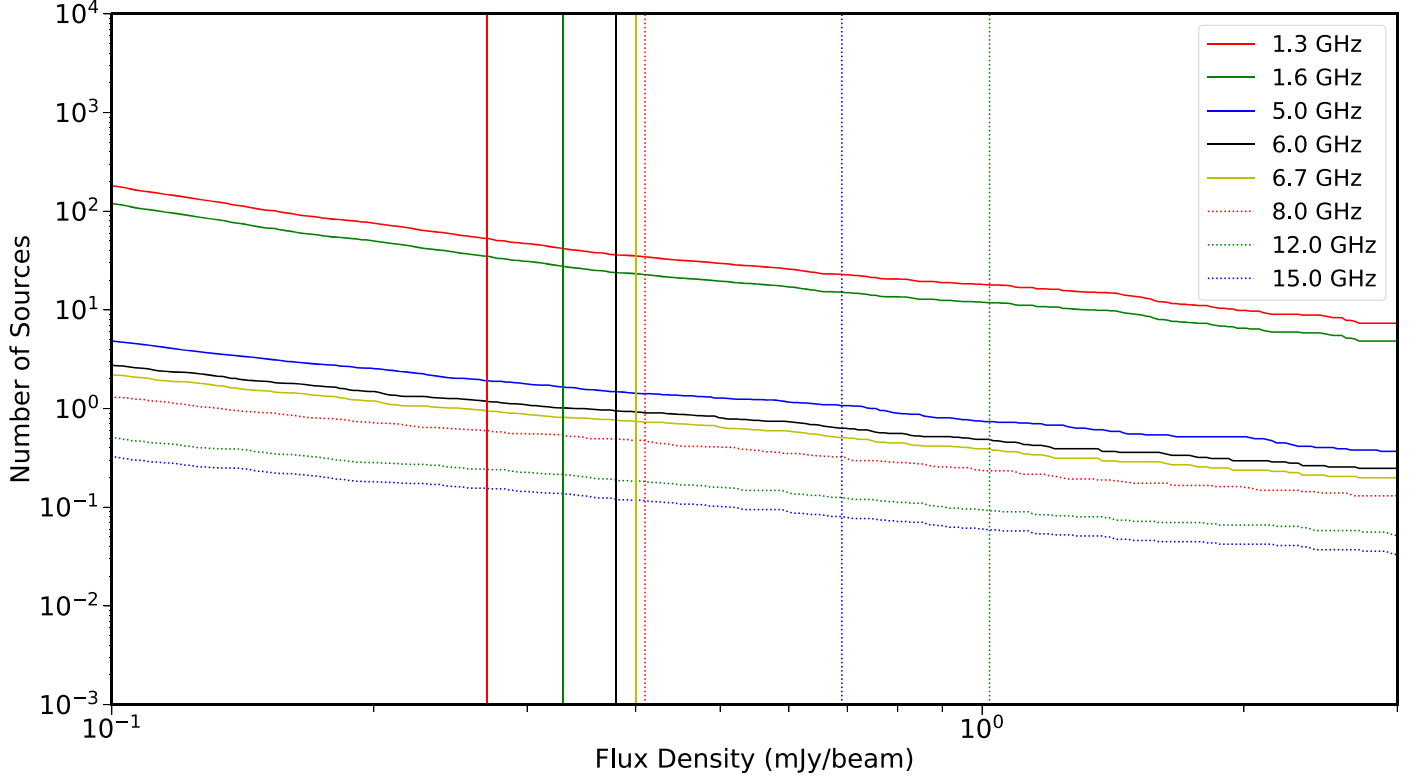
Figure 6. Number of in-beam sources. The vertical lines indicate the sensitivity matched DR of 100:1 (see ΔS values listed in Table 3), where the lines for 5 and 6 GHz overlap.

isolated, binary or multiple systems, primary objects plus a group of objects rotating around them, or even more complex systems (such as the MW). In addition, SKA-VLBI can also be used to test GR.

3.1. Astrometry of Isolated Objects

SKA-VLBI will provide an opportunity to study isolated stellar objects in different stages of star formation and evolution, e.g., star formation regions (SFRs), post-main-sequence stars (mainly asymptotic giant branch, AGB, stars), and pulsars (PSRs; e.g., the PSRπ and MSPSRπ campaigns; Deller et al. 2011; Vigeland et al. 2018). Because SFR studies focus on the formation and evolution of central stars, such systems are classified as isolated celestial systems rather than multiple systems. Masers, which have been found in SFRs and associated with AGB stars, serve as ideal targets for measuring parallaxes and proper motions, the key quantities of astrometry. For an example online database of masers, please see Ladeyschikov et al. (2019).[9] The current bottleneck of maser measurements using VLBI, such as with the VLBA, has limitations imposed by limited sensitivity.

3.1.1. Star Formation Regions

CH$_3$OH masers at 6.7 GHz were discovered by Menten (1991), which, along with 22.2 GHz H$_2$O masers, are the brightest and most widespread maser species in HMSFRs (e.g., Caswell et al. 1995; Minier et al. 2003; Xu et al. 2008). Sugiyama et al. (2013) conducted 6.7 GHz CH$_3$OH maser monitoring studies, using the EAVN to observe 36 target sources in HMSFRs. Fujisawa et al. (2014) subsequently released the results of this program, who found that maser emission was detected for 35 sources. This group published a detailed case study on the source G006.79-00.25, and found that 6.7 GHz CH$_3$OH maser spots were both rotating and expanding (Sugiyama et al. 2016). It is worth noting that Moscadelli et al. (2013) pointed out that 6.7 GHz maser emission traces gas entrained in the jet. In addition, Bartkiewicz et al. (2020) used the EVN to observe 6.7 GHz CH$_3$OH masers near the massive YSO G23.657-00.127, and concluded that it was hard to determine whether the methanol masers were tracing a spherical outflow arising from an (almost) edge on disk or a wide-angle wind at the base of a protostellar jet. SKA-VLBI will have high sensitivity and will be able to detect faint sources. Assuming an observation at 6.7 GHz with an integration time of 1 hr and a bandwidth of

---

[9] https://maserdb.net/

2 kHz, a 1σ would be possible at $\sim$1.4 mJy beam^{-1} (see Table 3), which is better than the $\sim$4 mJy beam^{-1} in Bartkiewicz et al. (2020). The estimated beam size ($\sim$0.9 mas) is also smaller than that in Bartkiewicz et al. (2020) by a factor of $\sim$7. These facts indicate it is very likely that more maser spots will be detected by SKA-VLBI, and the resulting astrometric precision will also improve. Combining search of radio continuum emission with high spatial resolution (such as by SKA-Mid) to pinpoint the driving source of the masers, SKA-VLBI is expected to discern between the scenarios of sphere-like outflow and wide angle wind at the base of the protostellar jet (see above, Bartkiewicz et al. 2020), i.e., distinguish which part of the outflowing gas near YSO is traced by 6.7 GHz CH$_3$OH masers. It is also possible to conduct further similar studies on more HMSFRs to determine statistically whether the scenario is unified for different sources.

Gould's Belt Distances Survey (GOBELINS) was dedicated to measuring the distances and proper motions of young stars in neighboring molecular clouds using VLBA at 5 and/or 8 GHz with a bandwidth of 256 MHz. Results from this survey have been reported for the Ophiuchus complex (Ortiz-León et al. 2017b), Orion molecular clouds (Kounkel et al. 2017), the Serpens/Aquila molecular complex (Ortiz-León et al. 2017a), and the Perseus molecular cloud (Ortiz-León et al. 2018). The dynamics of star formation and young stars within molecular clouds were studied. For binary or multiple young stars, physical properties such as mass and orbital parameters have also been published (for more details see Section 3.2.1). The typical sensitivity of GOBELINS was $\sim$25 μJy, which is far worse than the ΔS in Table 3, indicating that SKA-VLBI will be able to detect more younger stars (see also Ortiz-León et al. 2017b). Therefore, SKA-VLBI is expected to help compose a more complete picture of the synergistic study of young stars and molecular cloud dynamics.

In addition, it is interesting to note that in a case study of the Protostellar Outflows at the Earliest Stages (POETS) survey presented by Sanna et al. (2019), linearly polarized emission from 6.7 GHz CH$_3$OH masers was detected for G035.02+0.35, and the direction of the magnetic field was found to be consistent with the axis of the jet. It is expected that studies of the Zeeman effect in 6.7 GHz CH$_3$OH masers (e.g., Vlemmings 2008; Crutcher & Kemball 2019; Dall'Olio et al. 2020) of early stage protostars will further complement studies of their magnetic fields by using SKA-VLBI with its higher sensitivity. This will enable the study of the magnetodynamics of SFRs and the influence of magnetic fields on star formation.

3.1.2. Post-main-sequence Stars

The significance of multiband and multiepoch observations of post-main-sequence stars (e.g., AGB stars, red supergiant stars, etc.) is that they can be used to (i) investigate the astrochemistry of material that has been ejected into the interstellar medium (ISM); (ii) distinguish different maser pumping mechanisms (e.g., radiative or collisional pumping), and derive these physical properties accordingly in circumstellar envelopes (CSEs); (iii) study the late stages of stellar evolution; and (iv) probe the spatial structure and dynamics related to mass-loss processes and measure asymmetry in CSEs (see Reid & Honma 2014; Rioja & Dodson 2020). The study of these post-main-sequence stars mainly relies on observations of 22.2 GHz H$_2$O, 43.1, 42.8, 86.2, and 129.3 GHz SiO, 1612, 1665, and 1667 MHz OH masers, and others, which are used to measure parallaxes, proper motions, radial velocities, and light variations, and to determine the overlaps or offsets between masers of different transitions, ring sizes, and their temporal evolution (Reid & Honma 2014). The VLBI parallaxes of AGB stars can also be compared with Gaia parallaxes, which are used to constrain the Gaia parallax zero-point offset (see Section 3.1.4 for details), and to calibrate the period–luminosity relation derived from oxygen-rich Mira variables in the MW (Andriantsaralaza et al. 2022).

Below 15 GHz, OH masers are good tracers of AGB stars. OH masers at 1612 MHz are a great tracer of low- and intermediate-mass oxygen-rich evolved stars with long-period stellar pulsations (i.e., types of AGB stars). This type of evolutionary stage with strong 1612 MHz OH maser emission is exclusively attributed to OH/IR stars. Observations of OH/IR stars can be traced back to the 1980s (e.g., Herman & Habing 1985; van Langevelde et al. 1990; Lindqvist et al. 1992), and include large-scale sky surveys performed with the Australian Telescope Compact Array (ATCA) and VLA (Sevenster et al. 1997a, 1997b, 2001). Engels & Bunzel (2015) provided a database for querying known 1612, 1665, and 1667 MHz OH masers.[10] Combining The HI/OH/Recombination line (THOR) survey of the MW (Beuther et al. 2016, 2019) and follow-up observations by the Southern Parkes Large-Area Survey by the ATCA in Hydroxyl (SPLASH; Qiao et al. 2016, 2018, 2020), Uno et al. (2021) conducted 3D simulations of OH/IR stars traced by 1612 MHz OH masers in the Galactic disk. From these simulation data, and within a scale height of 150 pc, they found there may be $\sim$3990 OH/IR stars in the Galactic plane, for which they determined their kinematic distances.

Ionospheric residuals can be largely reduced using Multi-View, and a spatial resolution can reach $\sim$3.9 mas, thus rendering SKA-VLBI a suitable instrument for studying OH/IR stars traced by 1612 MHz OH masers. The specific technical methodology and scientific strategy for future SKA astrometric missions to study 1612 MHz OH masers is currently under development (see Orosz et al. 2014). Figure 7 features the distribution of $\sim$3990 OH/IR stars, and the results affirm that SKA-VLBI can measure, in theory, the parallaxes of about 34% (1345/3990) of OH/IR stars with a distance precision of

---

[10] See https://hsweb.hs.uni-hamburg.de/projects/maserdb/.

(a) All stars.   (b) Zoom-in of stars within a Galactic latitude of $|5°|$.
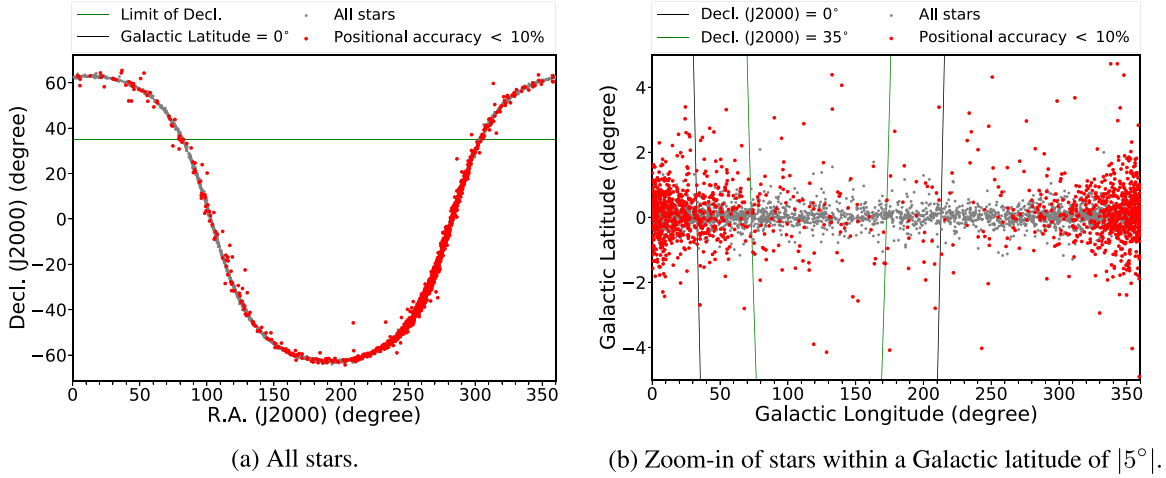
Figure 7. The distribution of OH/IR stars housing 1612 MHz OH masers from Uno et al. (2021), where the gray and red points present all OH/IR stars and stars with a theoretical parallax precision better than 10%, respectively. In the left panel, the black line represents a Galactic latitude of $0°$, and the green line indicates the decl. (J2000) limit of SKA-VLBI, i.e., $35°$. In the right panel, the black and green lines represent decl. (J2000) of $0°$ and $35°$, respectively.

better than 10% (here, we have assumed a bandwidth of 500 Hz, an integration time of 1 hr, the astrometric properties in Table 3, the highest parallax precision of 6 μas, and the maximum decl. (J2000) of $35°$). OH masers at 1665 and/or 1667 MHz can also be used to study AGB stars (e.g., van Langevelde et al. 2000; Vlemmings et al. 2003; Vlemmings & van Langevelde 2007).

3.1.3. Pulsars

Deller et al. (2011) proposed a major project to measure the parallaxes of pulsars (some of which are in binary systems), PSRπ, using VLBA. This project planned to observe 60 and 200 pulsars in its Phases I and II, respectively. Phase I was implemented over a 9 yr period (Deller et al. 2016, 2019) and the parallaxes and proper motions of 60 pulsars were obtained. The typical parallax precision was $\sim$45 μas, with the best being close to 10 μas, which was much more precise and accurate than a pulsar's dispersion measure (DM)-based distance (Chatterjee et al. 2009; Deller et al. 2009, 2019). It is worth noting that the astrometric errors of these near but weak sources are mainly determined by thermal noise (Rioja & Dodson 2020). Vigeland et al. (2018) reported a similar project, i.e., observing millisecond pulsars (which are highly probably in binary systems), MSPSRπ, using VLBA, and the parallaxes and proper motions of 18 millisecond pulsars were reported (Ding et al. 2020, 2023).[11]

In addition to measuring the parallaxes and proper motions of (millisecond) pulsars, a series of studies, including those related to projects PSRπ and MSPSRπ, have made great

progress obtaining the physical properties of pulsars, e.g., their effective temperature, radius, mass, and average electron density, and provided constraints on the time derivative of Newton's gravitational constant (e.g., Vigeland et al. 2018; Deller et al. 2019; Ding et al. 2020, 2021, 2023). This series of work has also contributed to the development of pulsar timing array (PTA) studies, such as providing accurate distances to pulsars, improving PTA sensitivity, and verifying and improving pulsar timing solutions (Madison et al. 2013; Vigeland et al. 2018; Deller et al. 2019). At the same time, pulsars provide a rich laboratory for studying nuclear and particle physics (Lorimer 2008; Deller et al. 2011); they can be used to test GR (Deller et al. 2009, 2018; Ding et al. 2021; Guo et al. 2021); they were used to find the first observational evidence for the existence of gravitational waves (Taylor & Weisberg 1989); and their study led to the discovery of the first exoplanet (Wolszczan & Frail 1992).

The advantages of MultiView are required for determining precise astrometry for pulsars, so that stronger sources with larger angular distances can be used as reference calibrators, providing commensurate precision (see Rioja & Dodson 2020). The high sensitivity of SKA-VLBI not only will enable the detection of weak sources while maintaining high DR, but it will also enable in-beam MultiView observations. In this section, the pulsar astrometry presented here is based on the assumption that astrometric precision is dominated by thermal noise. Herein, we consider the pulsar catalog provided by Manchester et al. (2005) and recently updated by Manchester et al. (2016), which contains 2536 pulsars. (Note that the pulsars published in PSRπ and MSPSRπ are also in this catalog.). Figure 8 shows the distribution of these pulsars, of which 12% (295/2536) have parallax and/or proper motion

---

[11] For the specific status of PSRπ and MSPSRπ, see https://safe.nrao.edu/vlba/psrpi/status.html.
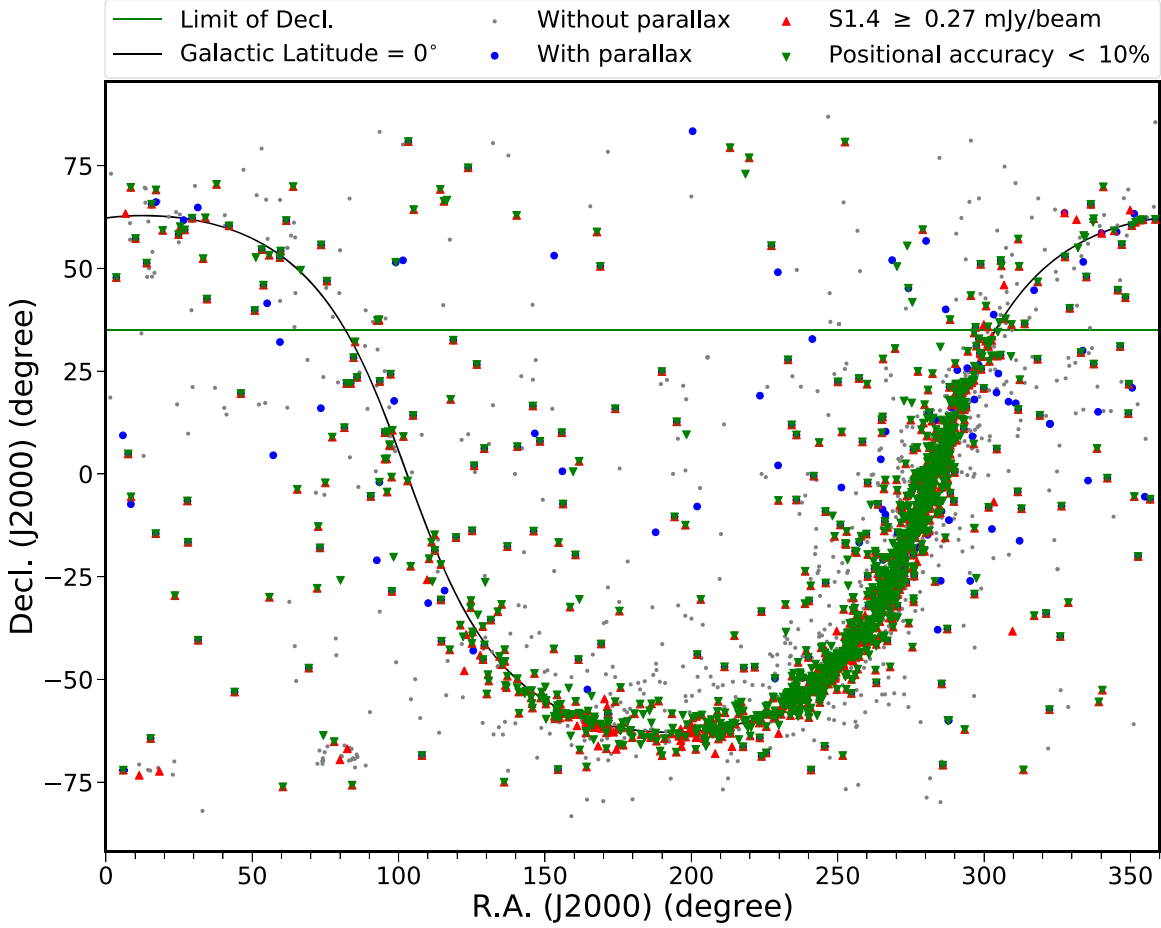
Figure 8. The distribution of pulsars from Manchester et al. (2016), where the gray and blue points represent pulsars with and without a parallax measurement, respectively. The red upper and green lower triangles indicate objects with flux densities at 1.4 GHz $\geqslant 0.27$ mJy beam^{-1} (i.e., the sensitivity matched to the DR of 100:1, see ΔS in Table 3) and objects with a theoretical parallax precision better than 10%, respectively. The black line signifies a Galactic latitude of 0°, and the green line indicates the decl. (J2000) limit, 35°, of SKA-VLBI.

measurements. In the catalog of Manchester et al. (2016), 1671 pulsars have flux density measurements (at 1.4 GHz), and 2481 have distance measurements (default is DM-based distance), but 864 have no flux density or distance measurements. According to the information in the catalog and the astrometric properties listed in Table 3, in theory, a total of ~48% (1225/2536) of these pulsars, located with a decl. (J2000) below 35°, can be measured with a distance precision better than 10%, and sources can be detected to 12.5 kpc (where the highest parallax precision is assumed to be ~8 μas, i.e., 1/3 of the astrometry precision listed in Table 3). There are 1014 pulsars whose flux densities are higher than the sensitivity matched to the DRs of 100:1 (i.e., $\geqslant 0.27$ mJy beam^{-1}) and decl. below 35°. Note that the observed DRs of pulsars can be enhanced when pulsar gating is applied in the correlator (see Deller et al. 2019; Ding et al. 2023). It is undeniable that SKA-VLBI astrometry with high sensitivity and high precision will be able to observe a large number of pulsars, making contributions to the measurement of electron density in the MW and the other science goals mentioned above.

3.1.4. Radio Stars: VLBI versus Gaia Parallaxes

Radio stars are stars visible in the radio band, which contain young stars, AGB stars, pulsars, etc. Multiepoch SKA-VLBI observations of radio stars can yield both high-precision astrometric parameters (such as parallax and proper motion) and high spatial resolution images. Combined with optical Gaia astrometry, the high-precision astrometry of SKA-VLBI can be used to link the optical and radio celestial reference frames, and verify the astrometric performance of VLBI and Gaia.

Long-term astronomical observations in both radio and optical bands can produce celestial reference frames, such as ICRF3 (Charlot et al. 2020) for radio and the Gaia DR2/(E) DR3 celestial reference frame (Gaia-CRF2/CRF3, which is
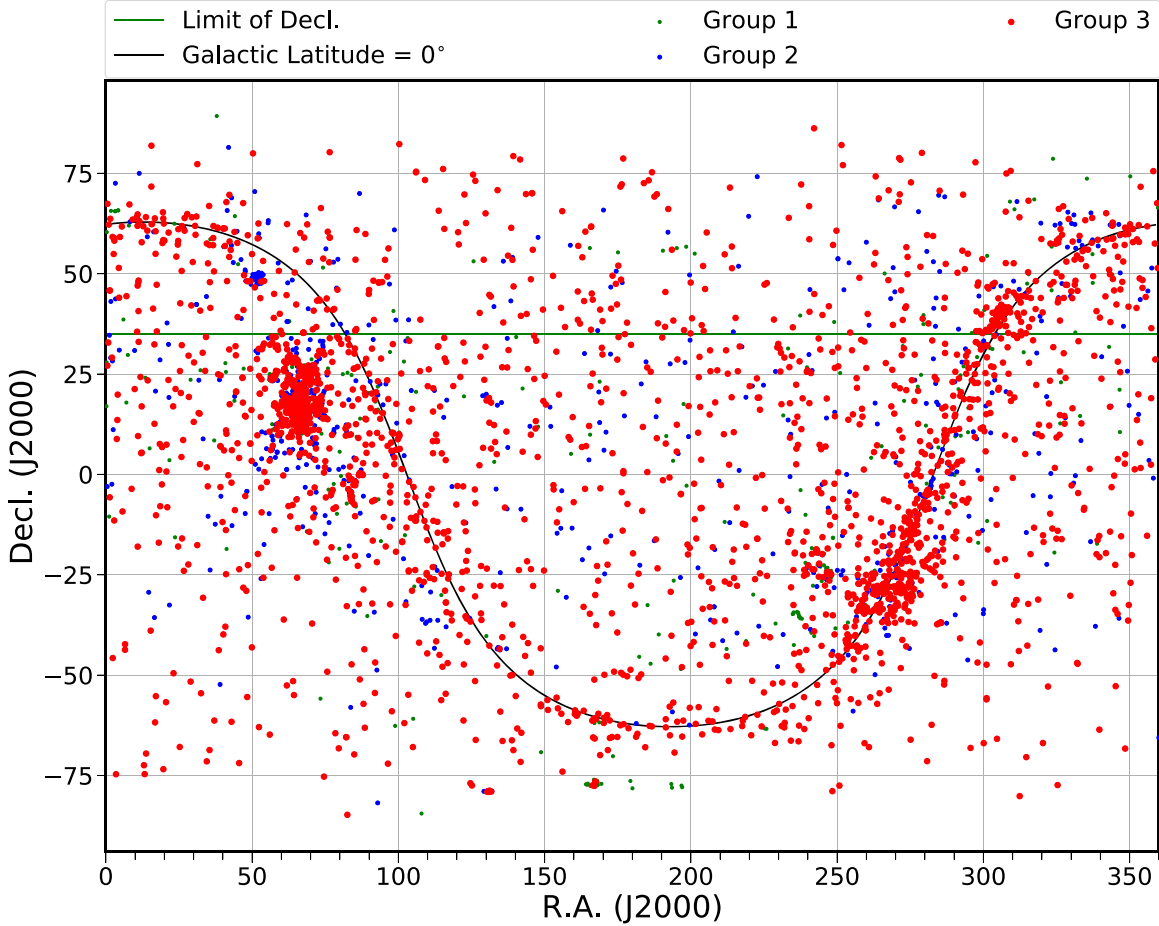
Figure 9. The distribution of radio stars from Wendker (1995), where the green points indicate all radio stars (Group 1), the blue points represent sources that had been observed at the frequencies considered in this work (Group 2), and the red points show sources whose flux densities (or upper limits) are higher than the sensitivity matched to the DR of 100:1 (Group3). The black line signifies a Galactic latitude of 0°, and the green line indicates the limiting decl. (J2000) of SKA-VLBI, i.e., 35°.

collectively called GCRF; Gaia Collaboration et al. 2018, 2022) in the optical. As mentioned previously, there are also notable VLBI-Gaia positional offsets (Mignard et al. 2016; Kovalev et al. 2017; Petrov & Kovalev 2017; Charlot et al. 2020; Liu et al. 2021; Secrest 2022). Observations of radio stars are helpful to tie together these international celestial reference frames (Reid & Honma 2014; Malkin 2016, for more details see Section 3.3.3).

It is interesting to compare the parallaxes of evolved AGB stars and other radio stars obtained with VLBI (i.e., such as the more than 130 stars used in the study by Xu et al. 2019) with those obtained with Gaia, as such a comparison offers a unique opportunity to test the Gaia parallax zero-point offset. Xu et al. (2019) compared the VLBI and Gaia parallaxes of their sample of stars and found that except for AGB stars, there was a systematic offset between the parallaxes, $-75 \pm 29 \, \mu$as, which was consistent with the zero-point offset of Gaia. For AGB stars, there was a significant difference between the Gaia and

VLBI parallaxes. Andriantsaralaza et al. (2022) compared the VLBI parallaxes of AGB stars with those of Gaia DR3 and obtained a zero-point offset of DR3 parallax of $\sim -77 \, \mu$as for bright AGB stars. They also found that the zero-point offset become more negative for fainter AGB stars, and Gaia DR3 underestimated the uncertainties of the parallaxes of these AGB stars.

Radio star astrometric observation plans were made in the latter part of the last century (e.g., Lestrade et al. 1986; Garrington et al. 1995; Lestrade et al. 1999; Johnston et al. 2003) and the early part of this century (e.g., Boboltz et al. 2003, 2007). Wendker (1995) provided a catalog of radio stars (note that the sample of radio stars discussed in this passage specifically refers to stars from this catalog) which is continually updated and currently contains 3699 stars (their distribution is displayed in Figure 9). These radio stars were observed at frequencies ranging from 20 MHz to 420 GHz, with 3230 stars falling within the SKA-VLBI frequency range

(which will be given priority in this work). SKA-VLBI will be able to measure precisely the parallaxes of radio stars whose flux densities (or upper limits) are higher than the sensitivity matched to the DR of 100:1 (only considering sources observed at 1.0–2.0 and 4.6–15.3 GHz which had a decl. (J2000) < 35°). The number of such radio stars is ~2033, which is about one order of magnitude higher than the number of radio stars that have reported VLBI parallaxes.

3.1.5. Other Isolated Objects

Matthews et al. (2023) reported the detection of 15 GHz continuous emission for the first time using VLA observations of a classic Cepheid, δ Cephei (δ Cep; distance of ~0.3 kpc), with a flux density ~15 μJy. For an integration time of 4 hr and a bandwidth of 1 GHz, the corresponding sensitivity of SKA-VLBI is ~1.8 μJy beam^{-1}. SKA-VLBI has the potential for direct triangular parallax measurements of classical Cepheids to be conducted, allowing astronomers to calibrate the period–luminosity relation more precisely. The theoretical distance precision is better than 10% for a classic Cepheid within 1.0 kpc assuming that its flux density at 0.3 kpc is ~15 μJy at 15 GHz (as in the case of δ Cep), where the assumed flux density is inversely proportional to the square of distance. Pietrukowicz et al. (2021) cataloged classical Cepheids in the MW, updated as of 2023,[12] and these classical Cepheids have been cross-matched with Gaia DR3 (Gaia Collaboration et al. 2023). There are over 3000 classical Cepheids in this catalog, with ~80 within ~1.0 kpc. Ripepi et al. (2023) provided a Gaia DR3 catalog of Cepheids containing some in neighboring galaxies, totaling over 15,000 Cepheids.

Combining high-precision VLBI astrometry and lunar ranging data, the mass of the Earth-Moon system and the Moon's moment of inertia ratio can be measured (see Lanyi et al. 2007; Reid & Honma 2014; Reid et al. 2019a). Combining VLBI data with optical observations, Doppler ranging data, and data from the Cassini satellite, the mass and potential of the Saturnian system were constrained (e.g., Jacobson et al. 2006). In addition, high-precision VLBI astrometry can also be used to monitor the trajectories of artificial radio sources (such as man-made spacecraft), contribute to geophysical research (such as measuring high-altitude winds, see Counselman et al. 1979; Sagdeyev et al. 1992; Reid & Honma 2014), and improve future space missions (see Duev et al. 2012). More research on satellite tracking can be found in the review by Reid & Honma (2014).

---

[12] See https://www.astrouw.edu.pl/ogle/ogle4/OCVS/allGalCep.listID.

3.2. Astrometry of Binary and Multiple Systems

3.2.1. Binary or Multiple Stellar Systems

Binary or multiple stellar systems include young binary or multiple stars, X-ray binaries (where one of the stars is a stellar black hole, a neutron star, or a white dwarf), Hulse-Taylor binary pulsar systems (HTBPSRs, which are composed of a neutron star and a pulsar, see Hulse & Taylor 1975), and other binary or multiple stellar systems containing neutron stars or black holes, cataclysmic variables (CVs, where the primary star is a white dwarf); see more details below. It is possible to monitor the orbital motions and measure the parallaxes, masses, orbital periods, and other physical quantities of these systems. The significance of studying binary or multiple stars includes testing theories of stellar structure and evolution; exploring star formation mechanisms and environmental effects in the galactic gravitational potential and in clusters; understanding important types of astrophysical phenomena such as Type Ia supernovae, CVs, and stellar X-ray sources (Horch 2013); testing fundamental physical theories such as the relativistic effects of binary/multiple stellar systems containing neutron stars and/or black holes (e.g., Deller et al. 2018; Ding et al. 2021; Guo et al. 2021); etc.

Younger binary or multiple stars. Orbital monitoring of young binary stars using VLA/VLBA has been carried out (e.g., Curiel et al. 2002; Loinard 2002; Rodríguez et al. 2003; Maureira et al. 2020, and GOBELINS, see Section 3.1.1). These studies provided orbital and other physical parameters of the binary/multiple-star systems. For example, Rodríguez et al. (2003) obtained the total mass and orbital period of the binary L1551 IRS 5 using the VLA, finding ~1.2 $M_\odot$ and ~260 yr respectively, while Maureira et al. (2020) combined VLA observations from Loinard (2002) and ALMA data to derive the mass range of the binary IRAS 16293–2422 A, finding $0.5 \lesssim M_1 \lesssim M_2 \lesssim 2\,M_\odot$. Using VLBA with its higher astrometric precision, GOBELINS also monitored the orbits of 17 young binary and nine young multiple stars, and obtained the orbital parameters for a total of 12 binary stars, including the mass of each single star in the binary system for nine systems. The maximum precision reached ~0.02 $M_\odot$ (corresponding to a relative precision up to better than 10%; see Ortiz-León et al. 2017a, 2017b; Kounkel et al. 2017; Ortiz-León et al. 2018). Among them, Ortiz-León et al. (2017b) even determined the mass of two stars in a triple-star system, YLW 12B. The value of $\theta_{\rm beam}$ at 5.0 GHz is ~1.2 mas (see Table 3), and the astrometric precision is better than 11 μas (assuming the flux density at 5 GHz is better than the minimum continuous emission of ~0.2 mJy in GOBELINS; Ortiz-León et al. 2017b, i.e., the matched DR is ~53:1, as shown in Table 3). Both of these are less than the semimajor axes of binary younger stars reported in GOBELINS (i.e., over ~10 mas). Therefore, the astrometric precision that may be obtained using SKA-VLBI

may be sufficient to conduct orbital monitoring of such binary and multiple star systems and more (see Section 3.1.1).

X-ray binaries. Some X-ray binaries have properties similar to quasars or other AGNs, but as they evolve much faster, they are often called microquasars. X-ray binaries can be used to study the interaction of stars with the accretion disks of the black holes or neutron stars they orbit, and to study the stability and lifetime of the corresponding jets; such approaches have been useful for studying the relativistic jets of distant quasars (Mirabel & Rodríguez 1998; Reynolds 2021). An important example of VLBI observation of an X-ray binary is Cygnus X-1 (Orosz et al. 2011; Reid et al. 2011; Miller-Jones et al. 2021); after obtaining the distance to this X-ray binary and monitoring its orbit, the mass-distance degeneracy in the simulation of optical/infrared data was broken, and the mass of the black hole and its companion star was therefore obtained. Several examples of X-ray binaries with measured parallaxes include Sco X-1, V404 Cyg, and Cygnus X-1 (see Fomalont et al. 2001; Miller-Jones et al. 2009; Reid et al. 2011), which were observed at frequencies of 1.7–22.2 GHz and their measured flux densities were $\gtrsim 5$ mJy beam^{-1}. It is expected that SKA-VLBI will be able to measure the parallaxes and semimajor axes of primary stars with a theoretical parallax precision of ~ 1 μas. It is also expected that SKA-VLBI will enable the exploration of fainter X-ray binaries and allow astronomers to monitor their light curves (e.g., Ng et al. 2024) with high sensitivity. Samples of X-ray binaries can be obtained from the Galactic high mass X-ray binary catalog (Neumann et al. 2023) and the Galactic low mass X-ray binary catalog (Avakyan et al. 2023).

HTBPSRs. An HTBPSR is a specific type of binary containing a pulsar (Hulse & Taylor 1975). Such binaries led to the first indirect detection of gravitational waves (see Taylor & Weisberg 1982, 1989) and can also be used to test GR (see Section 3.4.2 for details). An important representative is pulsar B1913+16, which has been studied extensively for many years. Weisberg & Taylor (2005) made an important review of studies of B1963+16, and since then there have been observations conducted by large radio telescopes and arrays (e.g., Arecibo and VLBA; Nice et al. 2005; Deller et al. 2018) and analyses of long-term observational data (e.g., Weisberg & Huang 2016). Weisberg & Huang (2016) obtained the ratio of the observed to GR-predicted orbital period decay rate (ROPR hereafter) of B1913+16 due to gravitational wave damping, 0.9983 ± 0.0016, which tested GR with a precision of 0.2%. They also found that the result was also consistent with the GR-predicted value from the Shapiro gravitational propagation delay. Using eight epochs of observations made over 2 yr with VLBA, Deller et al. (2018) obtained the ROPR, finding a value of $1.005^{+0.001}_{-0.003}$, which was incongruous with that of Weisberg & Huang (2016) but with similar level of precision. Therefore, further radio VLBI observations with higher astrometric

precision than achieved for pulsar B1913+16 and observations toward more HTBPSRs (which may be fainter) are imperative. These, in conjunction with pulsar observations (see Section 3.1.3), will constitute an important area of focus for SKA-VLBI.

Cataclysmic variables. CVs are interacting binaries in which a white dwarf accretes material from a low-mass companion. CVs are valuable to test theories of the evolution of binary stars; however, it is difficult to obtain precise values of the masses and radii of each star in a CV (Knigge et al. 2011; Littlefair et al. 2024). VLBI detections of CVs are scarce (e.g., nova RS Ophiuchi by VLBA; O'Brien et al. 2006, see nova below). Recently, Jiang et al. (2024) reported an EVN detection of an AE Aquarii (AE Aqr)-type CV,[13] LAMOST J024048.51 +195226.9, which possesses the fastest known rotating white dwarf with a spin period of ~ 25 s. This paper reported only its equatorial coordinates and no other astrometric parameter. Its maximum flux density at 1.7 GHz was ~ 1.0 mJy, indicating a potential target for SKA-VLBI to explore.

Novae. A nova is also a kind of CV. A classical nova is an eruption event on the surface of an accreting white dwarf binary. In such an event, the typical released energy is $\sim 10^{38}$–10^{43} erg, and heavy elements inside a white dwarf are ejected into the ISM (Gallagher & Starrfield 1978; Gehrz et al. 1998; José & Hernanz 2007; Romano et al. 2017), implying novae have a significant impact on the ISMs. Currently, theory and observations of novae are not overly consistent, especially in terms of the ejecta masses of different subtypes of novae. Radio observations are an ideal tracer of ejecta masses, and have already made significant contributions to the study of novae, such as constraining the expanding ejecta and their morphologies, distances, shell masses, and kinetic energies (see the short review by Gulati et al. (2023)). Gulati et al. conducted a systematic search for novae with decl. $\leqslant 41°$ using Australian Square Kilometre Array Pathfinder (ASKAP), discovering four nova radio counterparts, and conducted follow-up observations using ATCA. Their results highlight ASKAP's ability to contribute to future radio research of novae. The maximum radio flux density of a nova is related to the ejected mass, M_{ej}. At 1 GHz, assuming $M_{\mathrm{ej}} \sim 5 \times 10^{-4}$ $M_{\odot}$, SKA-VLBI may, in theory, be able to locate sources within ~ 10 kpc with a precision of better than 10% (based on the astrometry in Table 3) and the maximum flux density, which is associated with the M_{ej} taken from Table 4 in Gulati et al. 2023.[14] Note that the assumed maximum flux density is inversely proportional to the square of the distance. If the values of M_{ej} are 5×10^{-5} and 5×10^{-6} $M_{\odot}$, the

---

[13] It is a subtype of intermediate polars, which are a subclass of CVs with a moderate magnetic field strength of $10^5 \lesssim B \lesssim 10^7$ G and a sufficiently fast spin rate.

[14] For example, the maximum flux density at 1.0 GHz for a nova at 0.8 kpc is ~ 37.71, ~ 5.98 and ~ 0.95 mJy for $M_{\mathrm{ej}} \sim 5 \times 10^{-4}$, $\sim 5 \times 10^{-5}$ and $\sim 5 \times 10^{-6}$ $M_{\odot}$, respectively.

corresponding distance becomes ∼6 and ∼3 kpc, respectively. In these cases, the corresponding mass of the white dwarf is ∼0.4–1.25 $M_\odot$ (Yaron et al. 2005; Gulati et al. 2023).

Electromagnetic counterparts to gravitational wave sources. Such sources correspond to the merger of two neutron stars (NSNS), or a neutron star and a black hole (NSBH). A correlation linking short gamma-ray bursts, kilonovae, and NSNS/NSBH merges can be found in Figure 1 of Fernández & Metzger (2016). Alexander et al. (2017) detected the electromagnetic counterpart of the binary neutron star merger detected by LIGO/Virgo, GW170817 (LIGO Scientific Collaboration & Virgo Collaboration 2017; Abbott et al. 2017) at 6–15 GHz with a flux density of several 100 μJy beam^{-1}. A superluminal motion of a relativistic jet with flux density of ∼50 μJy beam^{-1} at 4.5 GHz was subsequently reported by Mooley et al. (2018). The expected sensitivity of SKA-VLBI will reach several μJy beam^{-1} (see Table 3) for an integration time of 1 hr at those frequencies, where the physical scale corresponding to ∼0.8 mas at 100 Mpc is ∼1 pc. Therefore, SKA-VLBI will be able to make movies of expanding ejecta or jets of merging NSNSs or NSBHs. SKA-VLBI is also expected to witness the precession of super-massive black holes (SMBHs), and provide a unique way to obtain a resolved image of the electromagnetic counterpart of a gravitational wave event (Reid et al. 2019a).

Other binaries. In this section we consider a binary star 1.8 kpc away that is similar to IM Pegasi (IM Peg; HR 8703; see Fomalont & Reid 2004; Ransom et al. 2012). The semimajor axis of the primary star is ∼0.1 au, the orbital period is ∼25 days, and the flux density at 8.4 GHz is typically ∼10 mJy at a distance of 96.4 pc. In such a case, the astrometric precision would reach about 57 μas (where the flux density is assumed to be 29 μJy, i.e., inversely proportional to the square of the distance), corresponding to an angular radius of ∼0.1 au, which is similar to the assumed semimajor axis of the primary star. Therefore, it is expected that the SKA-VLBI will provide high-precision astrometry of binary star orbits, at least for binaries within a distance of ∼1.8 kpc. Table 5 in Schwarz et al. (2016) lists catalogs of binary stars, and Mason et al. (2001) cataloged over 100,000 binary stars. Radio stars or OH/IR stars can also be sources of binary stars.

3.2.2. Exoplanets and Dwarfs

The first exoplanets were discovered when precise timing measurements were conducted of the 6.2 ms pulsar PSR 1257 +12 using the Arecibo radio telescope (Wolszczan & Frail 1992). In that work, the pulsar was thought to be orbited by two or more planet-sized bodies with masses of at least 2.8 and 3.4 $M_\oplus$ (where $M_\oplus$ is the mass of Earth). Searching for exoplanets using VLBI dates back to the work of Lestrade et al. (1996), where observations over a 7.5 yr period excluded a Jupiter-mass planet orbiting at a radius of 4 au from the central star σ^2

CrB, with postfit residuals of <0.3 mas (Reid & Honma 2014). Subsequently, Guirado et al. (1997) observed the active K0 star AB Dor and their result indicated a companion with a mass of ∼0.1 $M_\odot$. Two projects which focused on planets and dwarfs, respectively, were subsequently conducted: the Radio Interferometric Planet Search (RIPL, Bower et al. 2009) and the Radio Interferometric Survey of Active Red Dwarfs (RISARD, Gawronski et al. 2013). The RIPL collaboration reported on studies of GJ 896A, and found that the upper limit of the companion of GJ 896A was 0.15 M_J (where M_J is the mass of Jupiter) with a semimajor axis of 2 au, where the precisions of the parallax and proper motion were 0.2 mas and 0.01 mas yr^{-1}, respectively (Bower et al. 2011).

Recently, Curiel et al. (2022) found that the mass and the orbital period are 2.3 M_J and 284.4 days, respectively, for the single planet of the main star (GJ 896A) of the binary, GJ 896AB, through orbital monitoring with VLBA, and optical and infrared data. However, it is still poorly understood for outer planetary systems (Reid et al. 2019a). Fortunately, Schwarz et al. (2016) cataloged binary or multiple star system containing exoplanets,[15] with a total of 217 candidates, and the Extrasolar Planets catalog[16] also lists 4000 planetary systems (Butler et al. 2006; Le Sidaner et al. 2007; Schneider et al. 2011). These objects can serve as pilot target sources for investigating exoplanets and potential dwarfs by using SKA-VLBI, which has a higher sensitivity than VLBA.

3.2.3. Central Black Hole Systems in Galaxies

The nearest SMBH is Sgr A* at the center of the MW. Monitoring pulsar orbits around Sgr A* with precision astrometry has allowed astronomers to measure and test GR effects (although the observational frequency needs to be greater than about 10 GHz due to interstellar scattering; Reid & Honma 2014). Reports of monitoring observations of pulsars near the GC include only PSR J1745-2900 (see Mori et al. 2013; Bower et al. 2015). It is an opportunity for SKA-VLBI to conduct orbital monitoring of more pulsars to test GR with high precision. In addition, measuring the proper motion of Sgr A* will allow astronomers to constrain the mass of Sgr A*, evaluate the Sun's orbital motion around the GC, such as its circular rotation speed, Θ_0, and constrain the mass density of SMBH candidates (see Reid et al. 1999; Reid & Honma 2014; Reid & Brunthaler 2020).

3.2.4. Other Multiple Systems

The distances to star clusters can also be determined by using VLBI to measure parallaxes. Although the emission from individual stars in a cluster is very weak, the sensitivity of SKA may allow astronomers to observe them (Fomalont & Reid

---

[15] See https://adg.univie.ac.at/schwarz/multiple.html.
[16] See http://exoplanet.eu/catalog/.

2004). At present, the famous and the only example of using VLBI to measure the distance of a star cluster is the Pleiades cluster, where Melis et al. (2014) measured a distance of 136.2 ± 1.2 pc, which suggested that the Hipparcos-measured distance to the Pleiades cluster (i.e., 120.2 ± 1.5 pc) was in error. At the same time, Melis et al. (2014) proposed that Gaia should identify the unrecognized error in the Hipparcos measurement and correct it. Indeed, Gaia DR2 measured a distance of 135.15 ± 0.43 pc, which ended the "Pleiades distance controversy" (Lodieu et al. 2019). The flux of member stars in the Pleiades cluster is around several 100 μJy at $\sim$8 GHz (see Melis et al. 2014). Assuming a flux density of 100 μJy, SKA-VLBI can also measure the parallax of this cluster with a theoretical precision of $\sim 7 \times 10^{-4}$, i.e., a distance error of $\sim$0.1 pc, where the adopted integration time and bandwidth are shown in Table 3. The high-sensitivity SKA-VLBI has the potential to measure precisely the parallaxes to many more stellar clusters hosting radio stars (see Section 3.1.4), and compare them with those determined by Gaia.

From a few detections of 6.7 GHz CH$_3$OH masers in external galaxies (only detected in the Large Magellanic Cloud and M31, and tentatively detected in Maffei 2), it has been found that they are likely located in star-forming regions (clusters) and have peak luminosities in the range $\sim$500–2.3 $\times 10^4$ Jy kpc^2 (Chen et al. 2022). Assuming a peak luminosity of 10^4 Jy kpc^2, the peak flux density of a 6.7 GHz CH$_3$OH maser 100 kpc away can reach $\sim$1 Jy. Therefore, it is expected that SKA-VLBI can be used to measure precisely the parallaxes and proper motions of external galaxies within 60 kpc using 6.7 GHz methanol masers as tracers (assuming a parallax precision of $\sim$1.7 μas, i.e., 1/3 of the astrometric precision shown in Table 3). If the parallax precision is $\sim$1/5 of astrometric precision (which is achievable), the distances of external galaxies whose parallaxes can be precisely measured can reach even $\sim$100 kpc.

For a more distant galaxy, its distance can be derived by measuring the proper motion of two or more target sources within it, and comparing them with the galaxy's rotation model after obtaining its inclination angle, which is known as the van Maanen experiment (van Maanen 1923; Fomalont & Reid 2004; Reid & Honma 2014). The distance to M33 (which is about 730 kpc) was measured using this method (Brunthaler et al. 2002, 2005, 2008). Two distant galaxies, M31 and Maffei 2 (with distances of $\sim$0.8 and $\sim$5.7 Mpc, respectively), have (tentative) detections of 6.7 GHz CH$_3$OH masers (see Sjouwerman et al. 2010; Chen et al. 2022). Therefore, 6.7 GHz CH$_3$OH masers may be a potential tracer to measure distances via the van Maanen experiment. Such measurements of proper motions and geometric distances of galaxies within the Local Group are helpful to understand the Local Group's history, present state and future (Brunthaler et al. 2008). By applying the measured distances of external galaxies using the van Maanen experiment to distances of standard candles (e.g.,

Cepheids, Type Ia supernovae, etc.) inside them, the accuracy of the cosmic distance ladder may be improved to 1% or better (Fomalont & Reid 2004), and thus improve the accuracy of H_0. The proper motions of galaxies can also be used to study galaxy evolution; for example, it may be possible to predict whether will M31 and its two satellite galaxies M33 and IC 10 collide with the MW in the future (e.g., Reid et al. 2019a).

3.3. Astrometry of Complex Systems

3.3.1. The Structure of the Milky Way

Determining the structure of the MW has long been a difficult task. In the past 20 yr, advances in astrometry have led to a clearer understanding of the structure of the MW, especially within 5 kpc of the Sun. Such progress is based on high-precision radio astrometry applied to obtain the triangular parallaxes of masers in HMSFRs, and optical Gaia parallaxes of neighboring stars and open clusters (Xu et al. 2018b, 2021b; Reid et al. 2019b; Hao et al. 2021; Hou 2021). Nevertheless, to this day, controversy remains regarding such basic facts as the existence of some spiral arms, the number of arms, and the size of the MW. The mainstream view of the structure of the MW is that it is a four-arm spiral galaxy extending from the GC to the outer regions, with some extra arm segments and spurs (see Georgelin & Georgelin 1976; Reid et al. 2019b). Xu et al. (2023) proposed a new paradigm where the MW has a multiple-arm morphology with two symmetrical arms in the inner parts and is split into four spiral arms through two nearly symmetric bifurcations (see Figure 10). This new model suggests the MW may be an ordinary galaxy, as only 2% of known multiple-arm galaxies have four inner arms, while 83% have only two inner arms (Xu et al. 2023).

The most effective solution to addressing the controversy regarding the spiral structure of the MW is to obtain more parallax measurements of masers in HMSFRs widely distributed in the MW, including in the southern sky and to regions beyond the GC, as well as improving the parallax precision of objects. Compared with Gaia, maser emission is not absorbed significantly by interstellar dust, and is an excellent tracer for the entire MW. SKA-Mid will be located in the Southern Hemisphere. SKA-VLBI can cover regions of the sky with decl. (J2000) $< 35°$ with a theoretical parallax precision up to $\sim$1.7 μas, which can compensate for the current scarcity of triangular parallax measurements of masers in the southern sky.

Figure 10 shows the distribution of 6.7 GHz CH$_3$OH masers [17] superposed on the newly determined multiple-arm structure of the WM. The black points indicate 91 masers that currently have a parallax measurement made by the

---

[17] The tracer of the spiral arm structure shown in Figure 10 is the 6.7 CH$_3$OH maser, because surveys of 12.2 GHz CH$_3$OH masers are mostly conducted toward regions where 6.7 GHz CH$_3$OH masers were detected, while 22 GHz H$_2$O masers are not considered in this work.
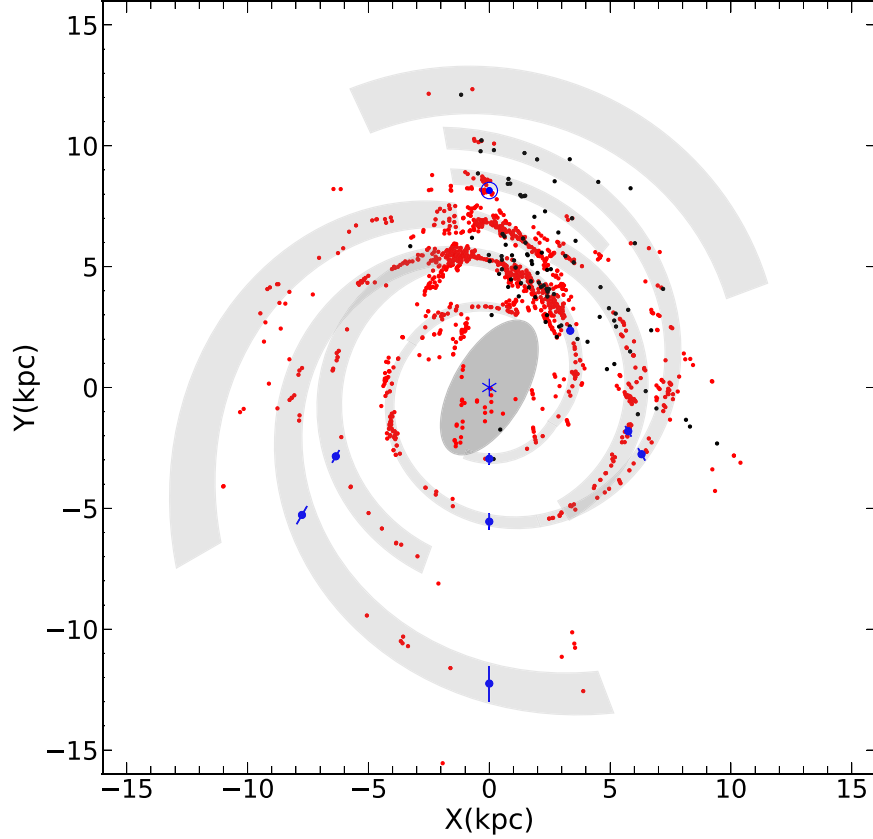
Figure 10. 6.7 GHz CH$_3$OH masers superposed on the multiple-arm structure (the gray patterns) of the WM determined by Xu et al. (2023), the ellipse indicates the bar following Hilmi et al. (2020). The GC (blue star) is at (0, 0) and the Sun (blue Sun symbol) is at (0, 8.15) kpc. The black points indicate the masers from the BeSSeL survey. The red points represent the other masers that can be observed by SKA-VLBI (i.e., decl. (J2000) $\leqslant 35°$), where the distance is calculated using the kinematic method. The blue dots and error bars show the assumptive sources with the parallax precision of 1.7 μas.

BeSSeL survey (Reid et al. 2019b; Xu et al. 2021a; Bian et al. 2022). The red points represent masers that can be observed by SKA-VLBI (i.e., decl. (J2000) $\leqslant 35°$), which include the catalog of Xu et al. (2009) and several other catalogs (with a large number of newly discovered masers) from 2008 onward, including the southern methanol maser sources observed by ATCA (Caswell 2009), the subsequent Methanol MultiBeam survey (Caswell et al. 2010, 2011; Green et al. 2010, 2012; Breen et al. 2015), the Torun catalog (Szymczak et al. 2012), and the survey conducted with the Tianma telescope (Yang et al. 2019). There are many masers located near the two bifurcations in the model of Xu et al. (2023), which would be a key sample to differentiate between this model and that of Reid et al. (2019b). To summarize, from this figure, SKA-VLBI is an ideal instrument to solve the controversy over the spiral structure of the MW (see above), and to map the relatively complete structure of the MW.

By comparing the spiral arm structures traced by masers with those traced by OB stars and open clusters obtained from Gaia astrometry, it is possible to study the consistency of the spiral arm structures traced by different young objects and the homogeneity of the distribution of star formation in the spiral arms (e.g., Xu et al. 2018a, 2021b). Naturally, we also expect SKA-VLBI to be able to observe the spiral arm structure depicted by other tracers, such as AGB stars (see Section 3.1.2), which can be compared with the results from Gaia astrometry to study the spiral arm structure traced by old objects (e.g., Poggio et al. 2021; Lin et al. 2022). It is also interesting to compare the spiral structure traced by old and young objects (e.g., Lin et al. 2022).

The parallaxes and proper motions of masers can also be used to study the structure, motion, and dynamics of spiral arms and the bar (e.g., Reid et al. 2019b; Immer et al. 2019; Li et al. 2022a); the dynamics in the central molecular zone (i.e., the central few 100 pc from the GC; e.g., Chambers et al. 2014; Kruijssen et al. 2015; Rickert 2017) and in the circumnuclear disk (e.g., Karlsson et al. 2003; Sjouwerman & Pihlström 2008) of the MW; and to measure the fundamental parameters of the MW. These parameters include R_0, Θ_0, the height of the Sun from the Galactic plane, $Z_\odot$, and the peculiar motion of the Sun

along the direction of its rotation, toward the GC, and the north pole, $(U_\odot, V_\odot, W_\odot)$, (e.g., Reid et al. 2014, 2019b; Xu et al. 2018b). Note that R_0 is a key parameter that directly affects measurements of the mass and luminosity of almost all objects in the MW (Bland-Hawthorn & Gerhard 2016). In addition, these parallaxes and proper motions can be used to derive the rotation curve of the MW, thus giving kinematic distance models (Reid et al. 2014, 2019b; Reid 2022). 3D motion in the vicinity of the solar system can be studied by combining the parallaxes and proper motions of HMSFR masers measured by VLBI and OB stars and young open clusters by Gaia, which produce a local velocity field and improve kinematic distance models (Liu et al. 2023).

3.3.2. Proper Motion Surveys of Extragalactic Systems

The expansion or contraction of the universe directly manifests itself as a change in the relative position between pairs of galaxies or galaxy clusters. Therefore, measuring the proper motions of galaxies or galaxy clusters can directly determine whether the universe is expanding or even accelerating, and subsequently the Hubble constant and the distance of galaxies (Darling 2013). For distant galaxies, the ideal target sources are AGNs. By measuring the proper motions of bright radio source pairs, Darling (2013) obtained inclusive 8.3 ± 14.9 μas yr^{-1} for small separation pairs (<200 Mpc, $z < 0.1$, where z is the redshift), which was not constrained enough to determine whether the universe was Hubble expanding or static. However, for large separation pairs (200–1500 Mpc), they obtained no net convergence or divergence for objects with $z < 1$, finding -2.7 ± 3.7 μas yr^{-1}, which is consistent with pure Hubble expansion and significantly inconsistent with a static universe. In order to determine further whether the relative proper motions of source pairs at distances <200 Mpc and $z < 0.1$ support Hubble expansion, more source pairs observed with higher astrometric precision and multiple observations of target sources are required. SKA-VLBI astrometry would be helpful to solve this issue.

Other applications of proper motion measurements of galaxies include measuring the secular aberration drift caused by the finite speed of light and the motion of the observer with respect to a light source; secular parallax, which is the motion of the solar system barycenter with respect to the cosmic microwave background (CMB) rest frame; the rotation of the reference frame; the anisotropic expansion of the universe; gravitational waves; large-scale structure; and baryon acoustic oscillation evolution; for more details see Darling et al. (2018). Secular aberration drift, aberration proper motion fields, and rotation are tightly tied to the ICRF, and affect the astrometry to all objects (Titov et al. 2011; Truebenbach & Darling 2017; MacMillan et al. 2019; Charlot et al. 2020).

Moreover, the peculiar velocity field on large scales at low redshift is a unique tracer to probe the dark matter density field, where peculiar velocities can be separated from recessional velocities due to the Hubble flow by using directly measured distances (Boruah et al. 2020). It is feasible to measure the distances to nearby galaxies with SKA-VLBI (see Section 3.2.4), and such measured distance can be used to determine the distances to Cepheids and Type Ia supernova inside those galaxies, and thus improve the precision of the cosmic distance ladder. It is also possible to obtain geometrical distances of extragalactic objects by using a large sample of extragalactic proper motions (Kardashev 1986; Ding & Croft 2009). In this method, it was suggested to use Earth's motion with respect to the CMB, which is $\sim$800 au over a 10 yr period, as a baseline to measure the proper motions of extragalactic objects. Assuming a positional precision of 2 μas, 10 yr of monitoring would achieve a theoretical precision of $\sim$0.2 μas yr^{-1}, and a measurable distance with an uncertainty of 20% could be reached for an object $\sim$80 Mpc distant with a baseline of 800 au using SKA-VLBI (see Figure 11). Chasing the 1 μas limit is exciting, as it can lead to measurable distances of galaxies as high as $\sim$160 Mpc.

3.3.3. Absolute Astrometry and the International Celestial Reference Frame

Absolute astrometry allows one to determine the true position of a radio source defined in a well-defined inertial frame (Fomalont & Reid 2004), e.g., the ICRF. The ICRF is a key problem in fundamental astrometry.

Since 1995, the VLBI-based ICRF (i.e., ICRF1, Ma et al. 1998) has been adopted as the IAU standard ICRF, including its second and third versions, ICRF2 and ICRF3, respectively (Fey et al. 2015; Charlot et al. 2020). At the same time, the optical celestial reference frame has also been constantly updated, such as the Hipparcos celestial reference frame (HCRF), and its successor, the GCRF based on Gaia DR2/(E)DR3 (Gaia Collaboration et al. 2018, 2022). Many comparisons between the VLBI-based ICRF and optical celestial reference frame have been made, resulting in the detection of VLBI-Gaia positional offsets (see Section 3.1.4). Among them, the noise floor of ICRF3 is $\sim$30 μas for individual source coordinates (Charlot et al. 2020), and the typical positional precision of sources in GCRF is $\sim$1 mas (Gaia Collaboration et al. 2022).

On the one hand, it is possible to solve the VLBI-Gaia positional offsets by improving the astrometric precision and spatial resolution of radio and optical observations, as well as obtaining more multiband observations and long-term monitoring of ICRF-defining sources. On the other hand, Froeschle & Kovalevsky (1982) proposed using radio stars to link the VLBI-based ICRF with optical celestial reference frames (e.g., HCRF and GCRF; see Kovalevsky et al. 1997; Malkin 2016).
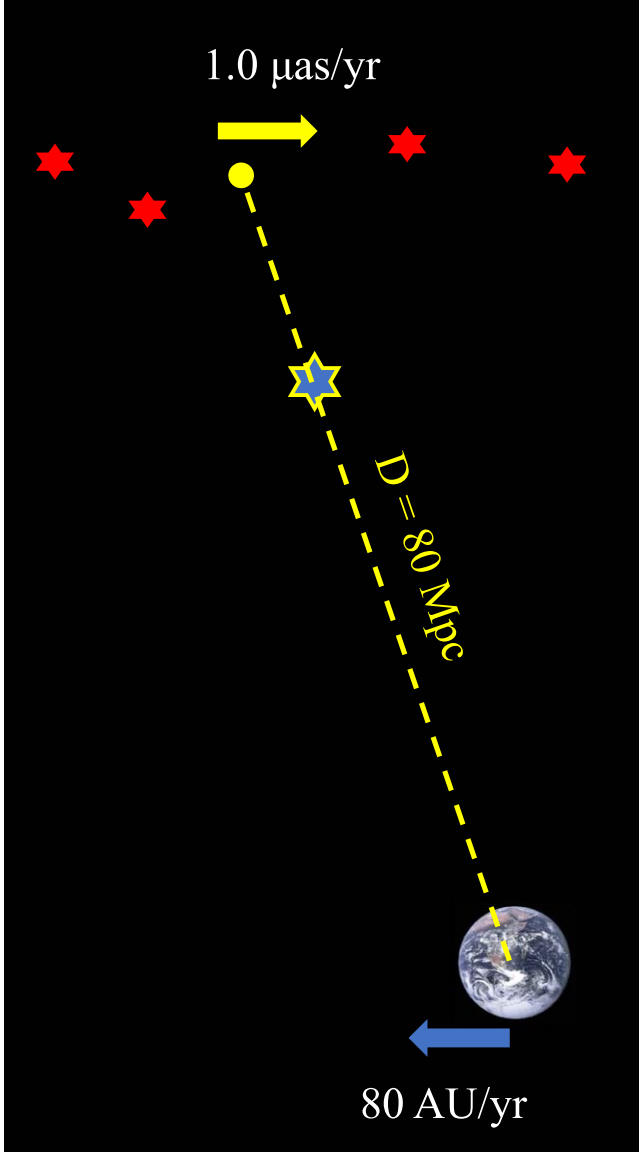
Figure 11. Schematic showing how geometrical distances can be obtained using Earth's motion with respect to the CMB as a baseline. In this model, no motion of an extragalactic object with respect to the CMB and the motion of the Earth of 80 au yr^{-1} with respect to the center of the CMB is assumed. With a theoretical proper motion precision of 0.2 μas yr^{-1} achievable through 10 yr of monitoring observations, the distance to an external galaxy 80 Mpc away could be determined with a $\sim$20% error (corresponding to a proper motion of 1.0 μas yr^{-1}). The icon of Earth is from the NASA/Apollo 17 crew, see https://www.nasa.gov/image-article/earth-full-view-from-apollo-17/.

This methodology is constantly improving and has achieved fruitful results (e.g., Malkin 2016; Lindegren 2020; Bobylev 2022; Chen et al. 2023). We have also presented the distributions of radio stars (see Section 3.1.4), OH/IR stars (see Section 3.1.2), and ICRF-defining sources in Figure 12, hoping to contribute to future links between GCRF and ICRF

using SKA-VLBI. Makarov et al. (2019) used radio-loud AGNs to link GCRF and ICRF and found that the Gaia DR2 parallax zero-point is color dependent (for the effect, see also Gaia Collaboration et al. 2021; Lindegren et al. 2021), suggesting an uncorrected instrumental calibration effect. Linking GCRF and ICRF helps to identify systematic errors in Gaia astrometry which can be corrected in future releases (Rioja & Dodson 2020).

It is possible to determine Earth's rotation and wobbles due to the influence of planets/other objects in the solar system as it orbits the Sun, by measuring the proper motion and/or parallax of Earth relative to an inertial coordinate system (e.g., ICRF; Fomalont & Reid 2004). The proper motion and parallax can also be used to investigate the motion of Earth's crust and its subsequent effect on ground-based telescopes, as well as other important information relevant for geophysical research.

The precision of the ICRF is important for improving the tracking precision of spacecraft, beacons, and satellite orbits and for determining planetary ephemerides. Planetary ephemerides are an important tool, which can be used to calculate the positions of celestial bodies in the solar system at any given time, be incorporated into VLBI data correlators, used for navigation, and employed to predict and/or backtrack astronomical phenomena (e.g., Li 2008). Determination of modern-day planetary ephemerides requires improving the precision of monitoring planets and their orbiting (artificial) satellites (e.g., Folkner et al. 2014; Pitjeva & Pitjev 2018; Fienga et al. 2020; Park et al. 2021). Linking planets to the ICRF through VLBI orbital monitoring of artificial satellites can also effectively improve their pointing uncertainties (e.g., Folkner & Border 2015; Park et al. 2021).

3.4. Tests of Relativistic Gravity and Gravitational Lenses

3.4.1. Solar System Tests of Relativistic Gravity

The celestial bodies in the solar system, which define the barycentric celestial reference system (BCRS) and act as gravitational sources, can play an important role in GR tests (for a review see chapter 8 of Ni 2017). There are several ways to conduct a solar system test of GR:

(1) Measure light deflection, the Shapiro time delay, and place constraints on the main parameter of parameterized post-Newtonian (PPN) formalism, γ.
(2) Measure relativistic perihelion advance and the solar quadrupole moment.
(3) Conduct ephemerides fitting.
(4) Measure time variability of the gravitational constant and mass loss from the Sun.
(5) Quantify frame-dragging effects.
(6) Conduct lunar laser ranging tests of relativistic gravity.

(a) Positional Accuracies from Table 3.

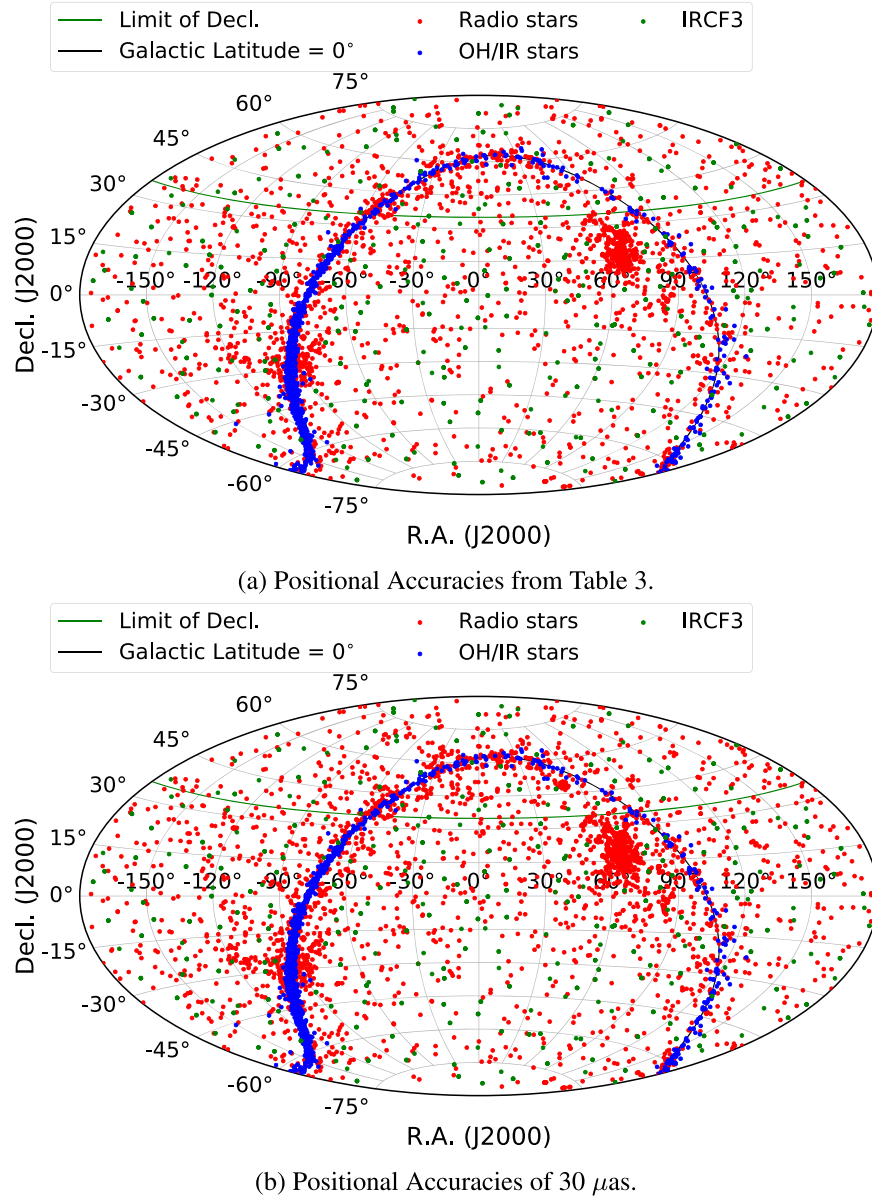(b) Positional Accuracies of 30 μas.

Figure 12. Distributions of radio stars (red points) and OH/IR stars (blue points) superposed on ICRF3-defining sources (green points). The green and black lines show the decl. (J2000) limit of SKA-VLBI (i.e., $<35°$) and a Galactic latitude of 0°, respectively. The criteria of the selected stars are that the flux density (or upper limit) matches the astrometric precision shown in Table 3 (panel (a)), and the astrometric precision is 30 μas (panel (b)), i.e., the noise floor in the individual source coordinates in ICRF3. For the OH/IR stars, only sources with a distance less than ~16 kpc are displayed. For the radio stars, only sources that had been observed at 1.0–2.0 and 4.6–15.3 GHz are presented.

SKA-VLBI will play an important role in at least points (1)–(5) above. For points (1) and (2), celestial bodies within the solar system act as gravitational sources. The role of SKA-VLBI in determining planetary ephemerides can be found in Section 3.3.3, while point (4) is often studied in conjunction with ephemerides fitting. SKA-VLBI can evaluate frame-dragging effects by measuring the proper motions of guide stars (for more details see the satellite mission Gravity Probe B (GP-B); Ratner et al. 2012; Shapiro et al. 2012, see also below).

Light deflection and the Shapiro time delay. The precision of γ obtained by measurements of light deflection and the Shapiro time delay has rapidly improved in recent years (for more details see the reviews by Will (2015); Thompson et al. (2017)). VLBI astrometry is an important technique that can lead to improved precision of γ. The precision of γ obtained using the VLBI technique has reached ~9×10^{-5} (Titov et al. 2018) where the Sun acts as a lens. Planets, such as Jupiter, have also been used to test GR using VLBI (e.g., Fomalont &

Kopeikin 2003, 2008; Li et al. 2022c) and data from Gaia EDR3/DR3 (see Abbas et al. 2022). Light deflection and the underlying theory (e.g., relativistic gravity, gravitational lensing theory, etc.) have become important tools for both astronomy and cosmology (Will 2015), while light deflection by solar system objects will pose a nonnegligible restraining factor in astrometry by SKA-VLBI, affecting positional accuracies at the level $\lesssim 1$ μas (Li et al. 2022b).

Taking the solar system planets as gravitational lenses, assuming a positional precision of 2 μas and there are ~ 250 sources within $2°$ (see Figure 6 at 15 GHz, where the FoV is set to be $\sim 2\rlap{.}'1$), and that light is deflected by ~ 2 mas caused by major planets (e.g., Jupiter), it is expected that 10 epochs of observations will produce a measurement precision for $\gamma \sim 10^{-6}$. If the Sun acts as a lens, the deflection angle of light $1°$ away from the Sun (which is favorable for successful observations; see Titov et al. 2018) can reach ~ 500 mas, and the number of sources within $1°$ is ~ 63. Therefore, the measurement precision of γ with 10 epochs of observations is expected to reach $\sim 10^{-8}$, achieving the advanced level in the next few decades (see chapter 8 in Ni 2017). In such a case, using measurements of light deflection caused by the gravitational fields of celestial bodies in the solar system via SKA-VLBI may allow astronomers to test the (noninertial) motion and multipole moment effect of celestial bodies, and test and develop second-order or higher PPN formalisms and/or different metric theories of gravity (e.g., Damour & Nordtvedt 1993; Kopeikin & Makarov 2007; Fomalont et al. 2009; Li et al. 2022c). More interestingly, measurements of light deflection may be able to test for the presence of dark energy in the solar system, which requires astrometric precision of $\lesssim 10$ μas (see Zhang 2022).

Relativistic perihelion advance. Another important component of solar system tests of GR is measuring the relativistic perihelion precession. This can be achieved by monitoring the orbits of planets or satellites in the solar system and measuring their annual precession. For example, for Mercury, the contribution of relativistic precession, $\Delta\phi$, is approximately 400 mas yr^{-1} (see page 1113 in Misner et al. 1973; Laskar & Gastineau 2009; Mogavero & Laskar 2021; Brown & Rein 2023). If the positional precision of SKA-VLBI will be 2 μas, the measurement precision of $\Delta\phi$ with 1 yr of monitoring can reach $\sim 5 \times 10^{-6}$. The relationship between $\Delta\phi$ and PPN parameters γ and β can be expressed by the following equation (see page 1116 in Misner et al. 1973)

$$\Delta\phi = \left[\frac{(2 - \beta + 2\gamma)}{3} \right] \left[\frac{6\pi GM_\odot}{c^2 a (1 - e^2)} \right] + J_2 \left[\frac{3\pi R_\odot^2}{a^2 (1 - e^2)^2} \right], \tag{6}$$

where G is the gravitational constant, $M_\odot$ and $R_\odot$ are the solar mass and radius, respectively, a and e are the semimajor axis

and the eccentricity of the orbit of Mercury, respectively, c is the speed of light, and J_2, the solar quadrupole moment, is $\sim 10^{-7}$ (see chapter 8 in Ni 2017). The second term is smaller than the first term by a factor of $\sim 6 \times 10^{-4}$, and the precision of J_2 can currently reach $\sim 10^{-2}$ (e.g., Pitjeva et al. 2022). Therefore, assuming a precision for γ of 10^{-6}, it is expected that SKA-VLBI will allow astronomers to test the PPN parameter β at a precision of $\sim 10^{-6}$. This precision will be comparable to the results obtained by fitting of Ephemerides of Planets and the Moon (EPM; e.g., 3×10^{-5} in Pitjeva 2013), allowing for mutual verification.

Ephemerides fitting and the time derivative of gravitational constant. As mentioned in Section 3.3.3, SKA-VLBI will likely play an important role in improving the precision of ICRF and planetary ephemerides. In fact, while fitting ephemerides, combined with orbital data of (artificial) satellites, GR can also be tested (such as the PPN parameters γ and β and the solar quadrupole moment, J_2); it may even be possible to obtain the time derivative of Newton's gravitational constant (e.g., Anderson et al. 2002; Fienga et al. 2011; Pitjeva 2013; Verma et al. 2014) and whether dark matter is present in the solar system (e.g., Pitjev & Pitjeva 2013; Pitjeva & Pitjev 2013); for more details see the review in chapter 8 in Ni (2017).

Frame-dragging effects. GP-B was a satellite mission that tested GR frame dragging, i.e., the Lense-Thirring effect, caused by the spin of Earth (see Ratner et al. 2012; Shapiro et al. 2012; Reid & Honma 2014). The task of VLBI in this research was to determine the proper motion of the guide star of the GP-B mission, the RS CVn binary IM Peg, i.e., -20.833 ± 0.090 mas yr^{-1} and -27.267 ± 0.095 mas yr^{-1} in R.A. and decl. (J2000), respectively. As mentioned previously for IM Peg in Section 3.2.1, SKA-VLBI will be capable of measuring its proper motion with a precision of ~ 4 μas yr^{-1}, thus improving the precision with which GR frame dragging can be tested. Moreover, the theoretically predicted Lense-Thirring effect signatures of the Galilean moons (such as Io, Europa, Ganymede, and Callisto) can, in principle, currently be detected with an astrometric precision of ~ 10 mas (Iorio 2023). The flux densities of these satellites were over ~ 10 mJy, as observed with the VLA at 15 GHz when Jupiter was ~ 4.46 au from Earth (de Pater et al. 1984). These flux densities are much higher than the sensitivity, ΔS, listed in Table 3 (i.e., 6.9 μJy beam^{-1}), indicating SKA-VLBI may be a suitable instrument to measure the Lense-Thirring effect on the Galilean moons of Jupiter.

3.4.2. Other Tests of the Relativistic Gravity

HTBPSRs can be used to test GR (see Section 3.2.1). The measurement of HTBPSR orbital decay depends heavily on the fundamental parameters of the MW (e.g., R_0 and Θ_0, see Section 3.3.1), where the acceleration of the Sun and pulsar in their Galactic orbits needs to be considered (for the Sun, Θ_0^2/R_0,

and for a pulsar, $\Theta^2(R)/R$; for more details see Reid & Honma 2014; Deller et al. 2018; Reid et al. 2019a). This orbital decay is caused by gravitational radiation, as predicted by GR (Damour & Taylor 1991); thus measuring such decay and deducting the impact of the acceleration of the Sun and pulsar in Galactic orbit provide further tests of GR. A series of studies of the classical HTBPSR, B1913+16, showed that VLBA observations of HTBPSRs can test GR with a precision of $\sim10^{-3}$ (Deller et al. 2018), but more HTBPSRs and more observations are required (see Section 3.2.1). If we keep the parameters in Deller et al. (2018) unchanged and simply replace their precision in parallax and proper motion by 6 μas and 19 μas yr^{-1} at L2 band, respectively, the calculated "Galactic" correction caused by kinematic effects, $\dot{P}_b^{\mathrm{gal}}$, to the observed orbital period derivative is $\dot{P}_b^{\mathrm{gal}} = -(0.008 \pm 0.001) \times 10^{-12}$ s s^{-1}, and the ROPR would be 1.0053 ± 0.0006, as determined by monitoring PSR B1913+16. The uncertainties of $\dot{P}_b^{\mathrm{gal}}$ and ROPR are about seven and four times lower than those reported in Deller et al. (2018), respectively. It is also expected that more precise values of R_0 and Θ_0 will result from higher-precision measurements of the parallaxes and proper motions of densely distributed HMSFRs in the MW (see Section 3.3.1), which may also lead to a more precise measurement of $\dot{P}_b^{\mathrm{gal}}$. Therefore, SKA-VLBI astrometry will be able to test GR with high precision by observing HTBPSRs. GR has also been tested by monitoring the orbital decay of pulsar binaries (e.g., composed of a pulsar and a white dwarf, Guo et al. 2021) and double neutron star binaries (e.g., Ding et al. 2021).

Monitoring pulsar orbits around Sgr A* at the GC can also allow astronomers to measure and test GR effects with high-precision astrometry (see Section 3.2.3; Reid & Honma 2014). GR can also be tested by measuring the proper motions of galaxies. The deflection of light from QSOs by a primordial gravitational wave background spanning 10^{-18}–10^{-8} Hz may also be measured or constrained using SKA-VLBI (see Gwinn et al. 1997; Book & Flanagan 2011; Truebenbach & Darling 2017).

3.4.3. Gravitational Lenses

Gravitational lenses, a variant of Einstein's light deflection, are an important tool in astronomical research (Will 2015). According to the shapes of images, gravitational lensing can be divided into weak and strong, where the former causes images to be weakly deformed, and the latter results in multiple images (see chapter 8 of Aharonian et al. (2013)). Gravitational microlensing can be thought of as a version of strong gravitational lensing, where the image separation is too small to be resolved (see part 4 in Schneider et al. 2006).

The application of strong gravitational lensing includes a natural telescope that magnifies galaxies or galaxy clusters, enhances the resolution of the instruments, and is beneficial for observing high redshift sources; studies of cosmology; reconstruction of the mass distribution of the lens; etc. Multiple images have the same intrinsic spectrum, structure, and polarization properties. The observed differences between images (such as spectrum and polarization) can be used to study different propagation effects, such as dust extinction and reddening, free–free absorption, and Faraday rotation in the radio regime (for more details see chapter 8 of Aharonian et al. 2013). Such properties can also be used to measure the Hubble constant (e.g., the series of works by the TDCOSMO collaboration; see Millon et al. 2020). Gravitational microlensing allows astronomers to study dark energy (see part 4 in Schneider et al. 2006), although its prominent application is to search for exoplanets, dwarfs, and dark stars (such as neutron stars, white dwarfs, stellar black holes, etc.; Mao & Paczynski 1991; Zhu & Dong 2021; Kaczmarek et al. 2022). Weak gravitational lensing allows astronomers to reconstruct the mass profile of the lensing galaxy or galaxy cluster, study the mass–luminosity relationship, trace the universal density profile, and study the geometric configuration of the universe (for more details see chapter 8 of Aharonian et al. 2013).

The advantage of radio VLBI observations of the lensing is that they can provide information at all scales from Mpc to pc, allowing astronomers to study the mass distribution of lenses. However, to date there have been few gravitational lenses detected in radio bands (see chapter 8 of Aharonian et al. 2013). Hartley et al. (2021) found signs of the existence of strong- or microlensing in radio images, which helped them study possible radio-quiet QSOs. Radio studies partially assisted by theoretical expectations have presented some possible hints of microlensing, but without clear detections (e.g., Lecavelier des Etangs et al. 2013; Vedantham et al. 2020). Radio research on weak lensing is also beginning to prosper, in the form of several current surveys (e.g., using VLA and/or e-MERLIN) and forthcoming surveys (using SKA; e.g., Chang et al. 2004; Harrison et al. 2016, 2020). However, it is still challenging to identify weak gravitational lensing events using current radio equipment such as VLA + e-MERLIN (e.g., Harrison et al. 2020), and there are not many resolved detections (Connor et al. 2022).

Koopmans et al. (2004) estimated that SKA will be able to detect 10^6 strong gravitational lensing events in a half-sky general-purpose survey, of which 10^5 could be easily detected. McKean et al. (2015) detailed the observing conditions, i.e., a θ_{beam} of $0''25$–$0''50$ and a depth of 3 μJy beam^{-1}. For Galactic black hole microlensing events, it may be possible to achieve a rate of ~10 yr^{-1} using VLBA with a flux limit of 3 μJy beam^{-1} (see Karami et al. 2016). For exoplanetary microlensing, phase I of SKA-Low may reach a rate of ~0.3 yr^{-1} or better (see Shiohira et al. 2020). The high-sensitivity SKA will allow for the measurement of weak gravitational lenses in the radio at a level comparable to optical surveys, suggesting its useful application in future weak lensing surveys (see, e.g.,

chapter 8 of Aharonian et al. 2013; Rivi et al. 2016; Connor et al. 2022). For example, SKA phase I may be comparable to optical stage III experiments such as the Dark Energy Survey (Bonaldi et al. 2016; Harrison et al. 2016; Camera et al. 2017). VLBI with SKA-Mid will also be competitive in cosmology studies, especially for ΛCDM cosmology, where auto-correlations and/or cross-correlation with galaxy weak-lensing and Lyα forest observations can be employed (e.g., Dash et al. 2023). SKA-VLBI will have a higher resolution compared to SKA, making it suitable for strengthening SKA surveys, and which has great potential to bring about a major breakthrough in gravitational lensing research.

It is worth mentioning that since light deflection caused by a gravitational field is independent of wavelength, gravitational lensing is generally achromatic. However, chromatic micro-lensing may also be important, e.g., the presence of important chromatic microlensing in strong lensed quasars (Kayser et al. 1986). One of the important origins of chromatic microlensing may be plasma, while others may be chromatic refractive deflection or selective absorption (for more details see Sun et al. 2023). Such phenomena, especially plasma lensing, have been studied in the radio band (e.g., Draine 1998; Bisnovatyi-Kogan & Tsupko 2017; Tsupko & Bisnovatyi-Kogan 2020), and will therefore be one of the potential subjects of SKA-VLBI.

4. Summary

SKA can form VLBI with telescopes on many continents, with baseline lengths mostly at ∼8000 km and above, and typical values of ∼10,000 km (Section 2.1). It is capable of achieving a beam size of several mas or below and an astrometric precision of several μas (Section 2.2) and sensitivity of several μJy (Table 3). The continued development of the AVN will be conducive to forming short and moderate baseline networks linked to SKA-Mid with better uv coverage, and complementing astrometry and mapping observations from dense to extended structures.

The astrometric sciences achievable with SKA-VLBI consist of:

1. *Astrometry of isolated objects (Section 3.1) and binary/multiple systems (Section 3.2), studying objects from star formation to the death of stars*. Those objects include protostars (Section 3.1.1), main-sequence stars (e.g., star HII 625 in the Pleiades open cluster; Section 3.2.4; Melis et al. 2014), evolved stars like AGB stars (Section 3.1.2), and pulsars (Section 3.1.3), white dwarfs and black holes (Section 3.2.1). For binary/multiple systems, monitoring their orbital motions may allow astronomers to derive their masses and other physical quantities (Section 3.2.1). Such studies can be extended down to planetary systems (Section 3.2.2) or up to systems surrounding the SMBHs at the centers of galaxies (Section 3.2.3), greatly

expanding the study of celestial bodies and celestial systems.

2. *Astrometry of complex systems, determining the structure of the MW, refining the ICRF, and enhancing surveys of AGNs or external galaxies.* To determine better the structure of the MW, observations covering both the Southern Hemisphere and part of the Northern Hemisphere are needed (Section 3.3.1) of objects. Theoretical effective observable distances of up to ∼100 kpc allow astrometry (e.g., parallax and proper motion) research to extend to possible nearby dwarf satellite galaxies (Section 3.2.4). Further refinement of the ICRF is needed (Section 3.3.3), including studies linking the radio and optical reference frames, perhaps by observing radio stars or radio-loud AGNs. SKA-VLBI will also enhance surveys of AGNs or other external galaxies (Section 3.3.2), allowing astronomers to investigate the expansion of the universe more precisely, constrain the Hubble constant, and facilitate studies on dark matter.

3. *Geometric distance ladder*. This ladder (which contains at least four components) can be formed from (1) direct trigonometric parallax measurements within the MW (e.g., masers in HMSFRs, Section 3.1.1; nearby classic Cepheids, Section 3.1.5; and stellar clusters, Section 3.2.4) and possible neighboring dwarf galaxies within ∼100 kpc (Section 3.2.4); (2) galactic distances estimated by possible comparisons of the proper motions of target sources inside galaxies with rotational models (Sections 3.2.4); (3) taking the Earth's motion with respect to the CMB as a baseline to measure the distances to galaxies (by measuring their proper motions; Section 3.3.2); and (4) using galaxy pair proper motion surveys to measure galactic distances statistically (Section 3.3.2). This geometric distance technique will cover scales from Earth sized up to a distance of ∼80 Mpc or above, providing a coverage range comparable to that from Cepheids to Type Ia supernovae in the cosmic distance ladder. Above all, this geometric distance ladder could provide diverse and independent calibration of the distances of standard candles in the cosmic distance ladder, yielding an independent method for determining the Hubble constant.

4. *Fundamental physics, including testing the theory of GR*. SKA-VLBI can be used to test the theory of GR in various ways and from various aspects, such as measuring light deflection caused by the gravitational fields of solar system objects and the perihelion precession of solar system objects (e.g., testing the PPN parameters γ and β at precision of order 10^{-8} and 10^{-6}, respectively); monitoring the orbits of solar system objects and studying their dynamics (for example, ephemerides fitting); and testing the GR frame drag caused by the rotation of Earth (Section 3.4.1). The by-

product of solar system tests of GR can be the study of dark matter and dark energy at these modest scales. Additionally, measuring the parallaxes and proper motions and/or orbital monitoring of HTBPSRs; pulsar binaries (with the companion being a white dwarf) or double neutral star binaries; and proper motion surveys of galaxies can also be used to test the theory of GR (see Sections 3.4.2).

5. *Synergy with optical astrometry*. Combining optical (e.g., Gaia) and radio astrometry can mutually verify the performance of both (see the example in Section 3.1.2), allowing astronomers to study the structure of the MW (Sections 3.3.1) and refine the ICRF (Section 3.3.3).

In summary, in addition to the abundant science goals discussed in this review, we eagerly anticipate hitherto unknown astrometric science with SKA-VLBI, undoubtedly derived from its high sensitivity and high precision.

Acknowledgments

Appendix
Telescope Properties and Possible SKA-VLBI Arrays

A total of 82 telescopes and/or tied arrays are listed in table A1 with their array name, e.g., VLBA, EVN (and its subarray MERLIN), EAVN (and its subarrays CVN, KVN, JVN, and VERA), LBA, SKA-Mid (SKA_M in the figures, and its pathfinders), and the code (which will appear frequently in this work), geographic longitude (λ) and latitude (φ), aperture (if it is an array, the number of dishes and the aperture of each dish are presented, separated by "$\times$"), minimum elevation (EL_{min}), and the SEFD in the L1, L2, C1, C2, C3, X, Ku1, and Ku2 bands, which are centered at 1.3, 1.6, 5.0, 6.0, 6.7, 8.0, 12.0, and 15.0 GHz (i.e., S_{L1}, S_{L2}, S_{C1}, S_{C2}, S_{C3}, S_X, S_{Ku1}, and S_{Ku2}), respectively. The corresponding URLs or references or other comments for each telescope are given in the last column.

Table A1
Potential Telescopes or Arrays that Could Form a VLBI Array with SKA-Mid

Arrays	Index	Telescope	Code	Aperture (m)	λ^a (°)	φ^a (°)	EL_{min} (°)	S_{L1} (Jy)	S_{L2} (Jy)	S_{C1} (Jy)	S_{C2} (Jy)	S_{C3} (Jy)	S_X (Jy)	S_{Ku1} (Jy)	S_{Ku2} (Jy)	References
VLBA	1	Saint Croix	VLBA_SC	25	−64.58	18.34	0	289	314	210	278	278	327	543	543	(1)
VLBA	2	Hancock	VLBA_HN	25	−71.99	43.07	0	289	314	210	278	278	327	543	543	(1)
VLBA	3	North Liberty	VLBA_NL	25	−91.57	42.31	0	289	314	210	278	278	327	543	543	(1)
VLBA	4	Fort Davis	VLBA_FD	25	−103.94	31.58	0	289	314	210	278	278	327	543	543	(1)
VLBA	5	Los Alamos	VLBA_LA	25	−106.25	36.31	0	289	314	210	278	278	327	543	543	(1)
VLBA	6	Pie Town	VLBA_PT	25	−108.12	37.33	0	289	314	210	278	278	327	543	543	(1)
VLBA	7	Kitt Peak	VLBA_KP	25	−111.61	32.06	0	289	314	210	278	278	327	543	543	(1)
VLBA	8	Owens Valley	VLBA_OV	25	−118.28	41.63	0	289	314	210	278	278	327	543	543	(1)
VLBA	9	Brewster	VLBA_BR	25	−119.68	56.59	0	289	314	210	278	278	327	543	543	(1)
VLBA	10	Maunakea	VLBA_MK	25	−155.46	20.25	0	289	314	210	278	278	327	543	543	(1)
VLA	11	phased VLA	VLA27	115	−107.62	34.08	8	16	14	12	12	12	10	12	12	(2)
GBT	12	GBT	GBT	110	−79.84	38.43	5	10	10	10	10	10	15	20	20	(3)
EVN/ MERLIN	13	Jodrell Bank-1	JOD1	76	−2.31	53.24	−1	35	40	70	80	80	...	...	...	(4)
EVN/ MERLIN	14	Jodrell Bank-2	JOD2	38 × 25	−2.31	53.24	0	9	5	8	8	8	...	...	...	(4)
EVN	15	Westerbork	WB_T	14 × 25	6.60	52.92	0	31	42	125	119	119	125	...	...	(4, 5)
EVN	16	Effelsberg	EFS	100	6.88	50.52	8	20	19	20	25	25	20	78	79	(6)
EVN	17	Medicina	MEDI	32	11.65	44.52	5	490	700	170	840	840	320	...	...	(4)
EVN	18	Noto	NOTO	32	14.99	36.88	5	740	740	260	1100	1100	840	...	...	(4)
EVN	19	Sardinia	SARD	65	9.25	39.49	5	67	67	...	50	50	...	...	...	(4)
EVN	20	Onsala	ONSA85	25	11.92	57.39	7	310	310	480	850	850	...	...	...	(4)
EVN	21	Onsala-60	ONSA60	20	11.93	57.40	6	...	...	...	...	...	785	...	...	(4)
EVN	22	Torun	TORU	32	18.56	52.91	2	250	300	220	650	650	...	...	...	(4)
EVN	23	Yebes	YEBE	40	−3.09	40.52	5	...	...	160	160	160	200	...	...	(4)
EVN	24	Irbene	IRBE	32	21.85	57.55	3	...	715	285	285	285	450	...	...	(4, 7)
EVN	25		IRBE16	16	21.85	57.56	3	...	...	623	558	569	651	...	...	(4, 8)
EVN	26	Metsähovi	METS	14	24.39	60.22	0	...	...	...	...	...	3200	...	...	(4)
EVN	27	Wettzell	WETT	20	12.88	49.15	0	...	...	...	...	...	750	...	...	(4)
EVN	28	Svetloe	SVET	32	29.78	60.53	−5	360	360	250	...	...	200	...	...	(4)
EVN	29	Zelenchukskaya	ZELE	32	41.57	43.79	3	300	300	330	...	...	200	...	...	(4)
EVN	30	Badary	BADA	32	102.23	51.77	−5	330	330	330	...	...	200	...	...	(4)
EVN/ MERLIN	31	Cambridge	CAMB	32	0.04	52.17	2	200	175	175	225	225	...	...	...	(4)
EVN/ MERLIN	32	Darnhall	MERLI1/ DARN	25	2.54	53.16	2	245[b]	250	188	188	188	...	...	...	(4)
EVN/ MERLIN	33	Defford	DEFF	25	2.14	52.10	2	350	350	1000	1600	1600	...	...	...	(4)
EVN/ MERLIN	34	Knockin	MERLI1/ KNOC	25	3.00	52.79	2	—[b]	—	—	—	—	...	...	...	(4)
EVN/ MERLIN	35	Pickmere	MERLI1/ TABL	25	2.45	53.29	2	—[b]	—	—	—	—	...	...	...	(4)
EVN	36	Robledo/DSS63	DSS63	70	−4.25	40.43	6	...	27	...	...	...	18	...	...	(4)
EVN	37	DSS65	DSSS	34	−4.25	40.43	6	...	...	...	...	...	61[c]	...	...	(4)
EVN	38	DSS-54	DSSS	34	−4.25	40.43	6	...	...	...	...	...	—[c]	...	...	(4)
EVN	39	DSS-55	DSSS	34	−4.25	40.43	6	...	...	...	...	...	—[c]	...	...	(4)
EVN	40	Matera	MATE	20	16.70	40.65	5	...	...	...	...	...	900	...	...	(9)

Arrays	Index	Telescope	Code	Aperture (m)	λ[a] (°)	φ[a] (°)	EL_{min} (°)	S_{L1} (Jy)	S_{L2} (Jy)	S_{C1} (Jy)	S_{C2} (Jy)	S_{C3} (Jy)	S_X (Jy)	S_{Ku1} (Jy)	S_{Ku2} (Jy)	References
EVN	41	Ny-Alesund	NYAL	20	11.87	78.93	2	...	...	...	...	...	1255	...	...	(4)
EVN/ CVN/ EAVN	42	Sheshan	SESHAN	25	121.14	31.09	8	...	670	720	1500	1740	800	...	...	(4, 10)
EVN/ CVN/ EAVN	43	Tianma	TIANMA	65	121.20	31.10	5	39	46	26	26	55	48	56	56	(4, 11)
EVN/ CVN/ EAVN	44	Nanshan	NANSH	26	87.18	43.47	5	300	300	250	...	...	350	...	...	(4, 10)
EVN/ CVN/ EAVN	45	Kunming	KUMI	40	102.80	25.03	8	...	...	350	290	307	480	...	...	(4, 10)
EVN/ KVN/ EAVN	46	KVN Yonsei	YSKVN	21	126.94	37.57	5	...	...	...	...	4241	...	...	...	(4, 10)
EVN/ KVN/ EAVN	47	KVN Ulsan	KUKVN	21	129.25	35.55	5	...	...	...	...	4241	...	...	...	(4, 10)
EVN/ KVN/ EAVN	48	KVN Tamna	KTKVN	21	126.46	33.29	5	...	...	...	...	4241	...	...	...	(4, 10)
EVN/ AVN/LBA	49	Hartebeesthoek	HART26	26	27.69	−25.89	10	...	430[d]	650	700	700	630	1175	...	(4, 12)
EVN/ AVN/LBA	50		HART15	15	27.67	−25.89	10	...	...	...	...	...	1400	...	...	(4, 12)
EAVN	51	Nobeyama	NOBE	45	138.47	35.94	12	...	...	...	...	...	...	...	...	(10)
EAVN	52	Takahagi	TAKA	32	140.69	36.70	5	...	...	...	...	200	...	...	...	(10)
EAVN	53	Hitachi	HITA	32	140.69	36.70	5	...	...	...	...	200	...	...	...	(10)
EAVN	54	Yamaguchi	YAMA	32	131.56	34.22	5	...	...	...	...	290	...	...	...	(10)
EAVN	55	Sejong	SEJO	22	127.30	36.52	0	...	...	...	...	...	...	...	...	(10)
EAVN/ VERA/JVN	56	Mizusawa	MIZU	20	141.13	39.13	5	...	...	...	...	2300	...	...	...	(10)
EAVN/ VERA/JVN	57	Iriki	IRIK	20	130.44	31.75	5	...	...	...	...	2300	...	...	...	(10)
EAVN/ VERA/JVN	58	Ogasawara	OGAS	20	142.22	27.09	5	...	...	...	...	2300	...	...	...	(10)
EAVN/ VERA/JVN	59	Ishigakijima	ISHI	20	124.17	11 24.41	5	...	...	...	...	2300	...	...	...	(10)
EAVN/JVN	60	Gifu	GIFU	11	136.74	35.47	10	...	...	...	...	...	...	...	...	(13, 14)
EAVN/JVN	61	Usuda	USUD	64	138.36	36.13	7	...	...	...	...	137	...	...	...	(13, 14)
LBA	62	ATCA/Narrabri	ATCA	6 × 22	149.57	−30.31	12	57	57	58	58	142	72	217	...	(15)
LBA	63	Mopra	MOPRA	22	149.07	−31.30	12	340	340	350	350	850	430	1300	...	(15)
LBA	64	Parkes	PARKS	64	148.26	−33.00	30	40	42	110	110	110	43	370	...	(15)
LBA	65	Tidbinbilla/DSS43	DSS43	70	148.98	−35.40	6	...	23	...	...	...	25	...	....	(15)

Table A1
(Continued)

Arrays	Index	Telescope	Code	Aperture (m)	λ[a] (°)	φ[a] (°)	EL_{min} (°)	S_{L1} (Jy)	S_{L2} (Jy)	S_{C1} (Jy)	S_{C2} (Jy)	S_{C3} (Jy)	S_X (Jy)	S_{Ku1} (Jy)	S_{Ku2} (Jy)	References
LBA	66	Tidbinbilla/DSS45	DSS45	34	148.98	−35.40	8	...	...	...	...	...	87	...	...	(15)
LBA	67	Hobart	HOBART26	26	147.44	−42.80	16	470	420	640	...	1240	560	1200	...	(15)
LBA	68		HOBART12	12	147.44	−42.80	10	...	...	3500	3500	3500	3400	3400	...	(16, 17)
LBA	69	Ceduna	CEDUNA	12	133.81	−31.87	20	...	...	450	...	550	600	750	...	(15)
LBA	70	Katherine	KATH	12	132.15	−14.40	10	...	...	3500	3500	3500	3400	3400	...	(16, 17)
LBA	71	Yarragadee	YARR	12	115.35	−29.00	10	...	...	3500	3500	3500	3400	3400	...	(16, 17)
LBA	72	Warkworth	WARK12	12	174.66	−36.40	7	...	...	3500	3500	3500	3400	3400	...	(18–20)
LBA	73		WARK30	30	174.66	−36.40	6	...	...	...	...	650	...	...	...	(18–20)
LBA/SKA	74	ASKAP	ASKAP	36 × 12	116.63	−26.70	15	70	80	...	...	...	...	...	...	(21, 22)
AVN/SKA	75	MeerKAT	MEER	64 × 13.5	21.44	−30.71	16	9[e]	...	...	...	...	...	...	...	(23)
AVN/SKA	76	SKA-Mid	SKA_M	133 × 15	21.44	−30.71	15	2.6[f]	2.6[f]	2.6[f]	2.6[f]	2.6[f]	2.6[f]	3.9[f]	3.9[f]	(24)
AVN	77	Ghana	GHAN	32	−0.31	5.75	0	...	...	563	...	563	...	...	...	(24–27)
CVN	78	Miyun	MIYU	50	116.98	40.56	5	...	...	...	...	...	227	...	...	(28)
...	79	FAST	FAST	500	106.86	25.65	50	2	...	...	...	...	...	...	...	(29–30)
...	80	uGMRT	GMRT	30 × 45	74.05	19.10	16	10	10	...	...	...	...	...	...	(31)
...	81	TNRO	TNRO	40	99.22	18.86	10	78	78	...	...	...	...	...	...	(32)
...	82	Jingdong	JING	120	101.00	24.50	5	6	6	6	6	6	...	...	...	(33)

Note.

[a] For telescopes in Europe, see https://www.craf.eu/radio-observatories-in-europe/, for others see column "References"

[b] We have represented the three telescopes in MERLIN as MERLIN1 because they are close to each other and their performances are similar.

[c] We have represented the three telescopes as DSSS because they are close to each other and their performances are similar.

[d] The minimum frequency is 1608 MHz.

[e] We only considered its L band, with frequency between 900 and 1670 MHz.

[f] Only consider the inner 4 km core (Paragi et al. 2015). We assume that all telescopes are equipped with receivers of all bands, but initially only a fraction of the telescopes will be equipped with Band 5 (i.e., 8300–15,300 MHz) receivers.

References. (1) https://science.nrao.edu/facilities/vlba; (2) https://science.nrao.edu/facilities/vla/docs; (3) https://www.gb.nrao.edu/scienceDocs; (4) http://old.evlbi.org/user_guide; (5) van Cappellen et al. (2022); (6) https://eff100mwiki.mpifr-bonn.mpg.de/doku.php; (7) https://www.virac.eu/en/research/technical-parameters; (8) Bleiders et al. (2017); (9) Colucci et al. (1999); (10) https://radio.kasi.re.kr/eavn/main.php; (11) http://radio-en.shao.cas.cn/facility/; (12) http://www.hartrao.ac.za/index.php; (13) http://astro.sci.yamaguchi-u.ac.jp/jvn/eng/status_e.html; (14) Wajima et al. (2016); (15) https://www.atnf.csiro.au/vlbi/; (16) Lovell et al. (2013); (17) Hyland et al. (2023); (18) Woodburn et al. (2015); (19) Petrov et al. (2015); (20) Weston et al. (2010); (21) https://www.atnf.csiro.au/projects/askap/index.html; (22) Hotan et al. (2021); (23) https://skaafrica.atlassian.net/wiki/spaces/ESDKB/pages/277315585/MeerKAT+specifications; (24) https://www.skao.int/en/science-users/; Paragi et al. (2015) (24) Duah Asabere et al. (2015); (25) de Witt et al. (2016); (26) Azankpo (2017); (27) Venter & Malan (2021); (28) Zhang et al. (2009); (29) Jiang et al. (2019); (30) Jiang et al. (2020); (31) http://www.ncra.tifr.res.in/ncra/gmrt; (32) Jaroenjittichai et al. (2022); (33) Wang et al. (2022).

References

Abbas, U., Bucciarelli, B., Lattanzi, M. G., et al. 2022, A&A, 664, A143

Abbott, B. P., Abbott, R., Abbott, T. D., et al. 2017, PhRvL, 119, 161101

Aharonian, F., Arshakian, T. G., Allen, B., et al. 2013, arXiv:1301.4124

Alexander, K. D., Berger, E., Fong, W., et al. 2017, ApJL, 848, L21

Anderson, J. D., Lau, E. L., Turyshev, S., Williams, J. G., & Nieto, M. M. 2002, AAS Meeting Abstracts, 200, 12.06

Andriantsaralaza, M., Ramstedt, S., Vlemmings, W. H. T., & De Beck, E. 2022, A&A, 667, A74

Avakyan, A., Neumann, M., Zainab, A., et al. 2023, A&A, 675, A199

Azankpo, S. 2017, Master's thesis, Stellenbosch University, South Africa

Bartkiewicz, A., Sanna, A., Szymczak, M., et al. 2020, A&A, 637, A15

Bessel, F. W. 1838, AN, 16, 65

Beuther, H., Bihr, S., Rugel, M., et al. 2016, A&A, 595, A32

Beuther, H., Walsh, A., Wang, Y., et al. 2019, A&A, 628, A90

Bian, S. B., Xu, Y., Li, J. J., et al. 2022, AJ, 163, 54

Bisnovatyi-Kogan, G., & Tsupko, O. 2017, Univ, 3, 57

Bland-Hawthorn, J., & Gerhard, O. 2016, ARA&A, 54, 529

Bleiders, M., Bezrukovs, V., & Orbidans, A. 2017, LatJP, 54, 42

Boboltz, D. A., Fey, A. L., Johnston, K. J., et al. 2003, AJ, 126, 484

Boboltz, D. A., Fey, A. L., Puatua, W. K., et al. 2007, AJ, 133, 906

Bobylev, V. V. 2022, AstL, 48, 790

Bonaldi, A., Bonato, M., Galluzzi, V., et al. 2019, MNRAS, 482, 2

Bonaldi, A., Harrison, I, Camera, S., & Brown, M. L. 2016, MNRAS, 463, 3686

Book, L. G., & Flanagan, É. É. 2011, PhRvD, 83, 024024

Boruah, S. S., Hudson, M. J., & Lavaux, G. 2020, MNRAS, 498, 2703

Bower, G. C., Bolatto, A., Ford, E. B., & Kalas, P. 2009, ApJ, 701, 1922

Bower, G. C., Bolatto, A., Ford, E. B., et al. 2011, ApJ, 740, 32

Bower, G. C., Deller, A., Demorest, P., et al. 2015, ApJ, 798, 120

Braun, R., Bourke, T., Green, J. A., Keane, E., & Wagg, J. 2015, Advancing Astrophysics with the Square Kilometre Array (AASKA14), 174

Breen, S. L., Fuller, G. A., Caswell, J. L., et al. 2015, MNRAS, 450, 4109

Brown, G., & Rein, H. 2023, MNRAS, 521, 4349

Brunthaler, A., Reid, M., Falcke, H., Greenhill, L. J., & Henkel, C. 2002, in Proc. of the 6th EVN Symp., Towards Proper Motions in the Local Group, ed. E. Ros, R.W Porcas, A.P Lobanov, & J.A Zensus (Bonn: The Max-Planck-Institut für Radioastronomie), 189

Brunthaler, A., Reid, M. J., Falcke, H., Greenhill, L. J., & Henkel, C. 2005, Sci, 307, 1440

Brunthaler, A., Reid, M. J., Falcke, H., Henkel, C., & Menten, K. M. 2008, in A Giant Step: from Milli- to Micro-arcsecond Astrometry, ed. W. J. Jin, I. Platais, & M. A. C. Perryman, 248 (Cambridge: Cambridge Univ. Press), 474, A Giant Step: from Milli- to Micro-arcsecond Astrometry M. A. C. M. A. C. M. A. C.

Brunthaler, A., Reid, M. J., Menten, K. M., et al. 2011, AN, 332, 461

Butler, R. P., Wright, J. T., Marcy, G. W., et al. 2006, ApJ, 646, 505

Camera, S., Harrison, I., Bonaldi, A., & Brown, M. L. 2017, MNRAS, 464, 4747

Caswell, J. L. 2009, PASA, 26, 454

Caswell, J. L., Fuller, G. A., Green, J. A., et al. 2010, MNRAS, 404, 1029

Caswell, J. L., Fuller, G. A., Green, J. A., et al. 2011, MNRAS, 417, 1964

Caswell, J. L., Vaile, R. A., Ellingsen, S. P., Whiteoak, J. B., & Norris, R. P. 1995, MNRAS, 272, 96

Chambers, E. T., Yusef-Zadeh, F., & Ott, J. 2014, A&A, 563, A68

Chang, T.-C., Refregier, A., & Helfand, D. J. 2004, ApJ, 617, 794

Charlot, P., Jacobs, C. S., Gordon, D., et al. 2020, A&A, 644, A159

Chatterjee, S., Brisken, W. F., Vlemmings, W. H. T., et al. 2009, ApJ, 698, 250

Chen, W., Zhang, B., Zhang, J., et al. 2023, MNRAS, 524, 5357

Chen, X., Yang, T., Ellingsen, S. P., McCarthy, T. P., & Ren, Z.-Y. 2022, ApJ, 926, 48

Clark, T. A., Hutton, L. K., Marandino, G. E., et al. 1976, AJ, 81, 599

Colucci, G., Del Rosso, D., & Vespe, F. 1999, Matera CGS VLBI Station, IVS 1999 Annual Report, 70

Condon, J. J. 1997, PASP, 109, 166

Connor, L., Bouman, K. L., Ravi, V., & Hallinan, G. 2022, MNRAS, 514, 2614

Counselman, C. C., Gourevitch, S. A., King, R. W., Loriot, G. B., & Prinn, R. G. 1979, Sci, 205, 85

Crutcher, R. M., & Kemball, A. J. 2019, FrASS, 6, 66

Crutcher, R. M., Wandelt, B., Heiles, C., Falgarone, E., & Troland, T. H. 2010, ApJ, 725, 466

Curiel, S., Ortiz-León, G. N., Mioduszewski, A. J., & Sanchez-Bermudez, J. 2022, AJ, 164, 93

Curiel, S., Trinidad, M. A., Cantó, J., et al. 2002, ApJL, 564, L35

Dall'Olio, D., Vlemmings, W. H. T., Lankhaar, B., & Surcis, G. 2020, A&A, 644, A122

Damour, T., & Nordtvedt, K. 1993, PhRvD, 48, 3436

Damour, T., & Taylor, J. H. 1991, ApJ, 366, 501

Darling, J. 2013, ApJL, 777, L21

Darling, J., Truebenbach, A., & Paine, J. 2018, in ASP Conf. Ser. 517, Science with a Next Generation Very Large Array, ed. E. Murphy (San Francisco, CA: ASP), 813

Dash, C. B. V., Sarkar, T. G., & Sarkar, A. K. 2023, JApA, 44, 5

de Pater, I., Brown, R. A., & Dickel, J. R. 1984, Icarus, 57, 93

de Witt, A., Mayer, D., MacLeod, G., et al. 2016, New Horizons with VGOS in International VLBI Service for Geodesy and Astrometry 2016 General Meeting Proceedings, ed. D. Behrend, K. D. Baver, & K. L. Armstrong, 118

Deller, A. T., Brisken, W. F., Chatterjee, S., et al. 2011, in European VLBI Group for Geodesy and Astronomy, PSRπ: A large VLBA pulsar astrometry program, ed. W. Alef, S. Bernhart, & A. Nothnagel, 178

Deller, A. T., Goss, W. M., Brisken, W. F., et al. 2019, ApJ, 875, 100

Deller, A. T., Tingay, S. J., Bailes, M., & Reynolds, J. E. 2009, ApJ, 701, 1243

Deller, A. T., Vigeland, S. J., Kaplan, D. L., et al. 2016, ApJ, 828, 8

Deller, A. T., Weisberg, J. M., Nice, D. J., & Chatterjee, S. 2018, ApJ, 862, 139

Ding, F., & Croft, R. A. C. 2009, MNRAS, 397, 1739

Ding, H., Deller, A. T., Fonseca, E., et al. 2021, ApJL, 921, L19

Ding, H., Deller, A. T., Freire, P., et al. 2020, ApJ, 896, 85

Ding, H., Deller, A. T., Stappers, B. W., et al. 2023, MNRAS, 519, 4982

Draine, B. T. 1998, ApJL, 509, L41

Duah Asabere, B., Gaylard, M., Horellou, C., Winkler, H., & Jarrett, T. 2015, arXiv:1503.08850

Duev, D. A., Molera Calvés, G., Pogrebenko, S. V., et al. 2012, A&A, 541, A43

Ellingsen, S. P. 2006, ApJ, 638, 241

Engels, D., & Bunzel, F. 2015, A&A, 582, A68

ESA 1997, ESA Special Publication, Vol. 1200, ESA Special Publication, 1200 (Noordwijk, Netherlands: ESA Publications Division)

Eubanks, T. M 1991, in Proceedings of the U.S. Naval Observatory Workshop on Relativistic Models for use in Space Geodesy (Washington, DC: U.S. Naval Observatory)

Fernández, R., & Metzger, B. D. 2016, ARNPS, 66, 23

Fey, A. L., Gordon, D., Jacobs, C. S., et al. 2015, AJ, 150, 58

Fienga, A., Avdellidou, C., & Hanuš, J. 2020, MNRAS, 492, 589

Fienga, A., Laskar, J., Kuchynka, P., et al. 2011, CeMDA, 111, 363

Fish, V. L., & Reid, M. J. 2006, ApJS, 164, 99

Fish, V. L., & Reid, M. J. 2007, ApJ, 670, 1159

Fish, V. L., Reid, M. J., Argon, A. L., & Zheng, X.-W. 2005, ApJS, 160, 220

Folkner, W. M., & Border, J. S. 2015, HiA, 16, 219

Folkner, W. M., Williams, J. G., Boggs, D. H., Park, R. S., & Kuchynka, P. 2014, IPNPR, 1, 42

Fomalont, E., Kopeikin, S., Lanyi, G., & Benson, J. 2009, ApJ, 699, 1395

Fomalont, E., & Reid, M. 2004, NewAR, 48, 1473

Fomalont, E. B. 2005, in ASP Conf. Ser. 340, Future Directions in High Resolution Astronomy, ed. J. Romney & M. Reid (San Francisco, CA: ASP), 460

Fomalont, E. B., Geldzahler, B. J., & Bradshaw, C. F. 2001, ApJ, 558, 283

Fomalont, E. B., & Kopeikin, S. 2008, A Giant Step: from Milli- to Micro-arcsecond Astrometry, in Proceedings of the International Astronomical Union, IAU Symposium, Radio interferometric tests of general relativity Vol. 248, ed. W. J. Jin, I. Platais, & M. A. C. Perryman, 383, M. A. C.M. A. C.

Fomalont, E. B., & Kopeikin, S. M. 2003, ApJ, 598, 704

Froeschle, M., & Kovalevsky, J. 1982, A&A, 116, 89

Fujisawa, K., Sugiyama, K., Motogi, K., et al. 2014, PASJ, 66, 31

Gaia Collaboration, Brown, A. G. A., Vallenari, A., et al. 2016, A&A, 595, A2

Gaia Collaboration, Brown, A. G. A., Vallenari, A., et al. 2021, A&A, 649, A1

Gaia Collaboration, Klioner, S. A., Lindegren, L., et al. 2022, A&A, 667, A148
Gaia Collaboration, Mignard, F., Klioner, S. A., et al. 2018, A&A, 616, A14
Gaia Collaboration, Vallenari, A., Brown, A. G. A., et al. 2023, A&A, 674, A1
Gallagher, J. S., & Starrfield, S. 1978, ARA&A, 16, 171
Garrington, S., Davis, R., Morrison, L., & Argyle, B. 1995, IEEES, 8, 7
Gawronski, M. P., Gozdziewski, K., & Katarzynski, K. 2013, arXiv:1309.4639
Gehrz, R. D., Truran, J. W., Williams, R. E., & Starrfield, S. 1998, PASP, 110, 3
Georgelin, Y. M., & Georgelin, Y. P. 1976, A&A, 49, 57
Green, J. A., Caswell, J. L., Fuller, G. A., et al. 2009, MNRAS, 392, 783
Green, J. A., Caswell, J. L., Fuller, G. A., et al. 2010, MNRAS, 409, 913
Green, J. A., Caswell, J. L., Fuller, G. A., et al. 2012, MNRAS, 420, 3108
Guirado, J. C., Reynolds, J. E., Lestrade, J. F., et al. 1997, ApJ, 490, 835
Gulati, A., Murphy, T., Kaplan, D. L., et al. 2023, PASA, 40, e025
Guo, Y. J., Freire, P. C. C., Guillemot, L., et al. 2021, A&A, 654, A16
Gwinn, C. R., Eubanks, T. M., Pyne, T., Birkinshaw, M., & Matsakis, D. N.
    1997, ApJ, 485, 87
Hao, C. J., Xu, Y., Hou, L. G., et al. 2021, A&A, 652, A102
Harrison, I., Brown, M. L., Tunbridge, B., et al. 2020, MNRAS, 495, 1737
Harrison, I., Camera, S., Zuntz, J., & Brown, M. L. 2016, MNRAS, 463, 3674
Hartley, P., Jackson, N., Badole, S., et al. 2021, MNRAS, 508, 4625
Herman, J., & Habing, H. J. 1985, A&AS, 59, 523
Hilmi, T., Minchev, I., Buck, T., et al. 2020, MNRAS, 497, 933
Høg, E., Fabricius, C., Makarov, V. V., et al. 2000, A&A, 355, L27
Horch, E. 2013, in Planets, Stars and Stellar Systems. Volume 4: Stellar
    Structure and Evolution, ed. T. D. Oswalt & M. A. Barstow, Vol. 4
    (Dordrecht: Springer), 653
Hotan, A. W., Bunton, J. D., Chippendale, A. P., et al. 2021, PASA, 38, e009
Hou, L. G. 2021, FrASS, 8, 103
Hulse, R. A., & Taylor, J. H. 1975, ApJL, 195, L51
Hyland, L. J., Reid, M. J., Orosz, G., et al. 2023, ApJ, 953, 21
Immer, K., Li, J., Quiroga-Nuñez, L. H., et al. 2019, A&A, 632, A123
Iorio, L. 2023, Univ, 9, 304
Jacobson, R. A., Antreasian, P. G., Bordi, J. J., et al. 2006, AJ, 132, 2520
Jaroenjittichai, P., Sugiyama, K., Kramer, B. H., et al. 2022, arXiv:2210.04926
Jiang, P., Cui, L., Liu, X., et al. 2024, MNRAS, 528, L112
Jiang, P., Tang, N.-Y., Hou, L.-G., et al. 2020, RAA, 20, 064
Jiang, P., Yue, Y., Gan, H., et al. 2019, SCPMA, 62, 959502
Johnston, K., de Vegt, C., & Gaume, R. 2003, AJ, 125, 3252
José, J., & Hernanz, M. 2007, JPhG, 34, R431
Kaczmarek, Z., McGill, P., Evans, N. W., et al. 2022, MNRAS, 514, 4845
Karami, M., Broderick, A. E., Rahvar, S., & Reid, M. 2016, ApJ, 833, 169
Kardashev, N. S. 1986, AZh, 63, 845
Karlsson, R., Sjouwerman, L. O., Sandqvist, A., & Whiteoak, J. B. 2003,
    A&A, 403, 1011
Kayser, R., Refsdal, S., & Stabell, R. 1986, A&A, 166, 36
Knigge, C., Baraffe, I., & Patterson, J. 2011, ApJS, 194, 28
Koopmans, L. V. E., Browne, I. W. A., & Jackson, N. J. 2004, NewAR,
    48, 1085
Kopeikin, S. M., & Makarov, V. V. 2007, PhRvD, 75, 062002
Kounkel, M., Hartmann, L., Loinard, L., et al. 2017, ApJ, 834, 142
Kovalev, Y. Y., Petrov, L., & Plavin, A. V. 2017, A&A, 598, L1
Kovalevsky, J., Lindegren, L., Perryman, M. A. C., et al. 1997, A&A, 323, 620
Kruijssen, J. M. D., Dale, J. E., & Longmore, S. N. 2015, MNRAS, 447, 1059
Ladeyschikov, D. A., Bayandina, O. S., & Sobolev, A. M. 2019, AJ, 158, 233
Lanyi, G., Bagri, D. S., & Border, J. 2007, IEEEP, 95, 2193
Laskar, J., & Gastineau, M. 2009, Natur, 459, 817
Le Sidaner, P., Dubernet, M. L., Simon, G., et al. 2007, in Proceedings of the
    Annual Meeting of the French Society of Astronomy and Astrophysics,
    Latest VO Development (V0-Paris Data Centre) ed. J. Bouvier,
    A. Chalabaev, & C. Charbonnel, 71
Lecavelier des Etangs, A., Sirothia, S. K., Gopal-Krishna, & Zarka, P. 2013,
    A&A, 552, A65
Lestrade, J.-F., Phillips, R. B., Jones, D. L., & Preston, R. A. 1996, JGR, 101,
    14837
Lestrade, J. F., Preston, R. A., Jones, D. L., et al. 1999, A&A, 344, 1014
Lestrade, J. F., Preston, R. A., Niell, A. E., Mutel, R. L., & Phillips, R. B. 1986,
    in Astrometric Techniques, Proceedings of IAU Symposium, Results of
    VLBI Observations of Radio Stars and Their Potential for Linking the
    HIPPARCOS and Extragalactic Reference Frames Vol. 109 (Dordrecht) ed.
    H. K. Eichhorn & R. J. Leacock, 779

Li, J. J., Immer, K., Reid, M. J., et al. 2022a, ApJS, 262, 42
Li, Y. 2008, ScChG, 51, 105
Li, Y., Xu, Y., Bian, S., et al. 2022b, ApJ, 938, 58
Li, Y., Xu, Y., Li, J., et al. 2022c, ApJ, 925, 47
LIGO Scientific CollaborationVirgo Collaboration 2017, GCN, 21509, 1
Lin, Z., Xu, Y., Hou, L., et al. 2022, ApJ, 931, 72
Lindegren, L. 2020, A&A, 633, A1
Lindegren, L., Bastian, U., Biermann, M., et al. 2021, A&A, 649, A4
Lindqvist, M., Winnberg, A., Habing, H. J., & Matthews, H. E. 1992, A&AS,
    92, 43
Littlefair, S. P., Rodríguez-Gil, P., Marsh, T. R., Parsons, S. G., &
    Dhillon, V. S. 2024, MNRAS, 527, 4353
Liu, D., Xu, Y., Hao, C., et al. 2023, ApJS, 268, 46
Liu, N., Lambert, S. B., Charlot, P., et al. 2021, A&A, 652, A87
Lodieu, N., Pérez-Garrido, A., Smart, R. L., & Silvotti, R. 2019, A&A,
    628, A66
Loinard, L. 2002, RMxAA, 38, 61
Lorimer, D. R. 2008, LRR, 11, 8
Lovell, J. E. J., McCallum, J. N., Reid, P. B., et al. 2013, JGeod, 87, 527
Ma, C., Arias, E. F., Eubanks, T. M., et al. 1998, AJ, 116, 516
Ma, C., Clark, T. A., Ryan, J. W., et al. 1986, AJ, 92, 1020
MacMillan, D. S., Fey, A., Gipson, J. M., et al. 2019, A&A, 630, A93
Madison, D. R., Chatterjee, S., & Cordes, J. M. 2013, ApJ, 777, 104
Makarov, V. V., Berghea, C. T., Frouard, J., Fey, A., & Schmitt, H. R. 2019,
    ApJ, 873, 132
Malkin, Z. 2016, MNRAS, 461, 1937
Manchester, R. N., Hobbs, G. B., Teoh, A., & Hobbs, M. 2005, AJ, 129, 1993
Manchester, R. N., Hobbs, G. B., Teoh, A., & Hobbs, M. 2016, yCat, 7245 B/
    psryCat
Mao, S., & Paczynski, B. 1991, ApJL, 374, L37
Marcaide, J. M., Shapiro, I. I., Corey, B. E., et al. 1985, A&A, 142, 71
Mason, B. D., Wycoff, G. L., Hartkopf, W. I., Douglass, G. G., &
    Worley, C. E. 2001, AJ, 122, 3466
Matthews, L. D., Evans, N. R., & Rupen, M. P. 2023, AJ, 165, 92
Maureira, M. J., Pineda, J. E., Segura-Cox, D. M., et al. 2020, ApJ, 897, 59
McKean, J., Jackson, N., Vegetti, S., et al. 2015, Advancing Astrophysics with
    the Square Kilometre Array (AASKA14), 84
Melis, C., Reid, M. J., Mioduszewski, A. J., Stauffer, J. R., & Bower, G. C.
    2014, Sci, 345, 1029
Menten, K. M. 1991, ApJL, 380, L75
Mignard, F., Klioner, S., Lindegren, L., et al. 2016, A&A, 595, A5
Miller-Jones, J. C. A., Bahramian, A., Orosz, J. A., et al. 2021, Sci, 371,
    1046
Miller-Jones, J. C. A., Jonker, P. G., Dhawan, V., et al. 2009, ApJL, 706, L230
Millon, M., Galan, A., Courbin, F., et al. 2020, A&A, 639, A101
Minier, V., Ellingsen, S. P., Norris, R. P., & Booth, R. S. 2003, A&A,
    403, 1095
Mirabel, I. F., & Rodríguez, L. F. 1998, Natur, 392, 673
Misner, C. W., Thorne, K. S., & Wheeler, J. A. 1973, Gravitation (New York:
    W.H. Freeman and Company)
Mogavero, F., & Laskar, J. 2021, A&A, 655, A1
Mooley, K. P., Deller, A. T., Gottlieb, O., et al. 2018, Natur, 561, 355
Mori, K., Gotthelf, E. V., Zhang, S., et al. 2013, ApJL, 770, L23
Moscadelli, L., Li, J. J., Cesaroni, R., et al. 2013, A&A, 549, A122
Neumann, M., Avakyan, A., Doroshenko, V., & Santangelo, A. 2023, A&A,
    677, A134
Ng, M., Hughes, A. K., Homan, J., et al. 2024, ApJ, 966, 232
Ni, W.-T. 2017, One Hundred Years of General Relativity: From Genesis and
    Empirical Foundations to Gravitational Waves, Cosmology and Quantum
    Gravity, 1 (Singapore: World Scientific)
Nice, D. J., Weisberg, J. M., & Taylor, J. H. 2005, AAS Meeting Abstracts,
    207, 183.05
O'Brien, T. J., Bode, M. F., Porcas, R. W., et al. 2006, Natur, 442, 279
Orosz, G., Dodson, R., Imai, H., et al. 2014, Testing methods for accurate OH
    maser astrometry, ATNF proposal id.V524, Semester: April, 2014
Orosz, J. A., McClintock, J. E., Aufdenberg, J. P., et al. 2011, ApJ, 742, 84
Ortiz-León, G. N., Dzib, S. A., Kounkel, M. A., et al. 2017a, ApJ, 834, 143
Ortiz-León, G. N., Loinard, L., Dzib, S. A., et al. 2018, ApJ, 865, 73
Ortiz-León, G. N., Loinard, L., Kounkel, M. A., et al. 2017b, ApJ, 834, 141
Paczynski, B. 2003, AcA, 53, 209

Paragi, Z., Godfrey, L., Reynolds, C., et al. 2015, Advancing Astrophysics with the Square Kilometre Array (AASKA14), 143
Park, R. S., Folkner, W. M., Williams, J. G., & Boggs, D. H. 2021, AJ, 161, 105
Perryman, M. 2012, EPJH, 37, 745
Petit, G., & Luzum, B. 2010, ITN, 36, 1
Petrov, L., & Kovalev, Y. Y. 2017, MNRAS, 471, 3775
Petrov, L., Natusch, T., Weston, S., et al. 2015, PASP, 127, 516
Pietrukowicz, P., Soszyński, I., & Udalski, A. 2021, AcA, 71, 205
Pitjev, N. P., & Pitjeva, E. V. 2013, AstL, 39, 141
Pitjeva, E., Pavlov, D., Aksim, D., & Kan, M. 2022, IAUS, 364, 220
Pitjeva, E. V. 2013, SoSyR, 47, 386
Pitjeva, E. V., & Pitjev, N. P. 2013, MNRAS, 432, 3431
Pitjeva, E. V., & Pitjev, N. P. 2018, CeMDA, 130, 57
Poggio, E., Drimmel, R., Cantat-Gaudin, T., et al. 2021, A&A, 651, A104
Qiao, H.-H., Breen, S. L., Gómez, J. F., et al. 2020, ApJS, 247, 5
Qiao, H.-H., Walsh, A. J., Breen, S. L., et al. 2018, ApJS, 239, 15
Qiao, H.-H., Walsh, A. J., Green, J. A., et al. 2016, ApJS, 227, 26
Ransom, R. R., Bartel, N., Bietenholz, M. F., et al. 2012, ApJS, 201, 6
Ratner, M. I., Bartel, N., Bietenholz, M. F., et al. 2012, ApJS, 201, 5
Reid, M., Loindard, L., Maccarone, T., & Melis, C. 2019a, BAAS, 51, 235
Reid, M. J. 2022, AJ, 164, 133
Reid, M. J., & Brunthaler, A. 2020, ApJ, 892, 39
Reid, M. J., & Honma, M. 2014, ARA&A, 52, 339
Reid, M. J., McClintock, J. E., Narayan, R., et al. 2011, ApJ, 742, 83
Reid, M. J., Menten, K. M., Brunthaler, A., et al. 2014, ApJ, 783, 130
Reid, M. J., Menten, K. M., Brunthaler, A., et al. 2019b, ApJ, 885, 131
Reid, M. J., Readhead, A. C. S., Vermeulen, R. C., & Treuhaft, R. N. 1999, ApJ, 524, 816
Reid, M. J., Schneps, M. H., Moran, J. M., et al. 1988, ApJ, 330, 809
Reynolds, C. S. 2021, ARA&A, 59, 117
Rickert, M. 2017, PhD thesis, Northwestern Univ.
Rioja, M. J., & Dodson, R. 2020, A&ARv, 28, 6
Ripepi, V., Clementini, G., Molinaro, R., et al. 2023, A&A, 674, A17
Rivi, M., Miller, L., Makhathini, S., & Abdalla, F. B. 2016, MNRAS, 463, 1881
Rodríguez, L. F., Curiel, S., Cantó, J., et al. 2003, ApJ, 583, 330
Romano, D., Matteucci, F., Zhang, Z. Y., Papadopoulos, P. P., & Ivison, R. J. 2017, MNRAS, 470, 401
Ryle, M., & Vonberg, D. D. 1946, Natur, 158, 339
Sagdeyev, R. Z., Kerzhanovitch, V. V., Kogan, L. R., et al. 1992, A&A, 254, 387
Sanna, A., Moscadelli, L., Goddi, C., et al. 2019, A&A, 623, L3
Schneider, J., Dedieu, C., Le Sidaner, P., Savalle, R., & Zolotukhin, I. 2011, A&A, 532, A79
Schneider, P., Kochanek, C. S., & Wambsganss, J. 2006, Gravitational Lensing: Strong, Weak and Micro (Berlin: Springer),
Schwarz, R., Funk, B., Zechner, R., & Bazsó, A. ´ 2016, MNRAS, 460, 3598
Secrest, N. J. 2022, ApJL, 939, L32
Sevenster, M. N., Chapman, J. M., Habing, H. J., Killeen, N. E. B., & Lindqvist, M. 1997a, A&AS, 122, 79
Sevenster, M. N., Chapman, J. M., Habing, H. J., Killeen, N. E. B., & Lindqvist, M. 1997b, A&AS, 124, 509
Sevenster, M. N., van Langevelde, H. J., Moody, R. A., et al. 2001, A&A, 366, 481
Shapiro, I. I., Bartel, N., Bietenholz, M. F., et al. 2012, ApJS, 201, 1
Shiohira, Y., Terada, Y., Mukuno, D., Fujii, Y., & Takahashi, K. 2020, MNRAS, 495, 1934
Sjouwerman, L. O., Murray, C. E., Pihlström, Y. M., Fish, V. L., & Araya, E. D. 2010, ApJL, 724, L158
Sjouwerman, L. O., & Pihlström, Y. M. 2008, ApJ, 681, 1287
Sugiyama, K., Fujisawa, K., Hachisuka, K., et al. 2013, ASP Conf. Ser. 476, New Trends in Radio Astronomy in the ALMA Era: The 30th Anniversary of Nobeyama Radio Observatory, ed. R. Kawabe, N. Kuno, & S. Yamamoto (San Francisco, CA: ASP), 347
Sugiyama, K., Fujisawa, K., Hachisuka, K., et al. 2016, PASJ, 68, 72

Sun, J., Er, X., & Tsupko, O. Y. 2023, MNRAS, 520, 994
Szymczak, M., Wolak, P., Bartkiewicz, A., & Borkowski, K. M. 2012, AN, 333, 634
Taylor, J. H., & Weisberg, J. M. 1982, ApJ, 253, 908
Taylor, J. H., & Weisberg, J. M. 1989, ApJ, 345, 434
Thompson, A. R., Moran, J. M., & Swenson, G. W., Jr. 2017, Interferometry and Synthesis in Radio Astronomy (3rd Edition; Berlin: Springer)
Titov, O., Girdiuk, A., Lambert, S. B., et al. 2018, A&A, 618, A8
Titov, O., Lambert, S. B., & Gontier, A. M. 2011, A&A, 529, A91
Truebenbach, A. E., & Darling, J. 2017, ApJS, 233, 3
Tsupko, O. Y., & Bisnovatyi-Kogan, G. S. 2020, MNRAS, 491, 5636
Uno, Y., Imai, H., Shinano, K., et al. 2021, MNRAS, 502, 3012
van Altena, W. F., Lee, J. T., & Hoffleit, E. D. 1995, The General Catalogue of Trigonometric [stellar] Parallaxes (New Haven, CT: Yale Univ. Observatory)
van Cappellen, W. A., Oosterloo, T. A., Verheijen, M. A. W., et al. 2022, A&A, 658, A146
van Langevelde, H. J., van der Heiden, R., & van Schooneveld, C. 1990, A&A, 239, 193
van Langevelde, H. J., Vlemmings, W., Diamond, P. J., Baudry, A., & Beasley, A. J. 2000, A&A, 357, 945
van Leeuwen, F. 2010, SSRv, 151, 209
van Maanen, A. 1923, ApJ, 57, 264
Vedantham, H. K., Callingham, J. R., Shimwell, T. W., et al. 2020, NatAs, 4, 577
Venter, M., & Malan, J. A. 2021, Radio Frequency Engineering Advancements for the Ghana Radio Telescope, in 2021 XXXIVth General Assembly and Scientific Symp. Int. Union of Radio Science (URSI GASS), 1–4
VERA Collaboration, Hirota, T., Nagayama, T., et al. 2020, PASJ, 72, 50
Verma, A. K., Fienga, A., Laskar, J., Manche, H., & Gastineau, M. 2014, A&A, 561, A115
Vigeland, S. J., Deller, A. T., Kaplan, D. L., et al. 2018, ApJ, 855, 122
Vlemmings, W. H. T. 2008, A&A, 484, 773
Vlemmings, W. H. T., & van Langevelde, H. J. 2007, A&A, 472, 547
Vlemmings, W. H. T., van Langevelde, H. J., Diamond, P. J., Habing, H. J., & Schilizzi, R. T. 2003, A&A, 407, 213
Wade, C. M., & Johnston, K. J. 1977, AJ, 82, 791
Wajima, K., Hagiwara, Y., An, T., et al. 2016, in ASP Conf. Ser. 502, Frontiers in Radio Astronomy and FAST Early Sciences Symp. 2015, ed. L. Qain & D. Li (San Francisco, CA: ASP), 81
Wang, M., Xu, Y., Wang, J., et al. 2022, SSPMA, 52, 119501
Weisberg, J. M., & Huang, Y. 2016, ApJ, 829, 55
Weisberg, J. M., & Taylor, J. H. 2005, in ASP Conf. Ser. 328, Binary Radio Pulsars, ed. F. A. Rasio & I. H. Stairs (San Francisco, CA: ASP), 25
Wendker, H. J. 1995, A&AS, 109, 177
Weston, S., Natusch, T., & Gulyaev, S. 2010, arXiv:1011.0227
Will, C. M. 2015, CQGra, 32, 124001
Wolszczan, A., & Frail, D. A. 1992, Natur, 355, 145
Woodburn, L., Natusch, T., Weston, S., et al. 2015, PASA, 32, e017
Xu, S., Zhang, B., Reid, M. J., Zheng, X., & Wang, G. 2019, ApJ, 875, 114
Xu, Y., Bian, S. B., Reid, M. J., et al. 2018a, A&A, 616, L15
Xu, Y., Bian, S. B., Reid, M. J., et al. 2021a, ApJS, 253, 1
Xu, Y., Hao, C. J., Liu, D. J., et al. 2023, ApJ, 947, 54
Xu, Y., Hou, L. G., Bian, S. B., et al. 2021b, A&A, 645, L8
Xu, Y., Hou, L.-G., & Wu, Y.-W. 2018b, RAA, 18, 146
Xu, Y., Li, J. J., Hachisuka, K., et al. 2008, A&A, 485, 729
Xu, Y., Li, J. J., Reid, M. J., et al. 2013, ApJ, 769, 15
Xu, Y., Reid, M., Dame, T., et al. 2016, SciA, 2, e1600878
Xu, Y., Reid, M. J., Zheng, X. W., & Menten, K. M. 2006, Sci, 311, 54
Xu, Y., Voronkov, M. A., Pandian, J. D., et al. 2009, A&A, 507, 1117
Yang, K., Chen, X., Shen, Z.-Q., et al. 2019, ApJS, 241, 18
Yaron, O., Prialnik, D., Shara, M. M., & Kovetz, A. 2005, ApJ, 623, 398
Zhang, B., Reid, M. J., Menten, K. M., et al. 2013, ApJ, 775, 79
Zhang, X.-Z., Zhu, X.-Y., Kong, D.-Q., et al. 2009, RAA, 9, 367
Zhang, Z. 2022, Classical Quantum Gravity, 39, 015003
Zhu, W., & Dong, S. 2021, ARA&A, 59, 291